Title
Glutamate-Leucine Block Copolypeptides for Drug Delivery

Author
Lee, Brian Sangwoo

Publication Date
2014

Peer reviewed|Thesis/dissertation

UNIVERSITY OF CALIFORNIA

Los Angeles

Glutamate-Leucine Block Copolypeptides for Drug Delivery

A thesis submitted in partial satisfaction

of the requirements for the degree Master of Science

in Bioengineering

by

Brian Sangwoo Lee

2014

ABSTRACT OF THESIS

Glutamate-Leucine Block Copolypeptides for Drug Delivery

by

Brian Sangwoo Lee

Master of Science in Bioengineering

University of California, Los Angeles, 2014

Professor Daniel T. Kamei, Chair

Chemotherapy treatments involving the delivery of naked drugs to the body must overcome many complications such as poor solubility, enzymatic degradation, and clearance from the body, all of which can result in the drug having a short circulation half-life, low efficacy, and undesirable side effects. One solution to overcome these problems is to encapsulate the drug within a nano-sized drug delivery vehicle. Nano-sized drug delivery vehicles are advantageous since they can protect the drug from degradation during its circulation in the body, release the drug in a controlled manner, and provide passive targeting to the tumor tissue.

Many materials for drug delivery vehicles have been investigated. Liposomes, which are vesicles composed of natural or synthetic phospholipids, have been thoroughly investigated, and many liposomal formulations have been successful in the market. However, one limitation of liposomes is that they are less stable due to being comprised of relatively smaller molecules that

exhibit weaker attractive interactions in a self-assembled vesicle. This disadvantage has motivated the development of other materials for drug delivery such as synthetic polymers, which are longer molecules that can exhibit stronger attractive interactions in a self-assembled vesicle. Synthetic control of the polymers also allows for fine tuning of the hydrophilic and hydrophobic chain lengths.

Another material that has been recently gaining popularity for use in drug delivery is the polypeptide. These amino acid-based building blocks provide further advantages. Similar to polymers, monodisperse polypeptides can be synthesized with precise control due to recent advances in polymerization techniques, and the longer chains provide stability for the self-assembled vesicles. They are also naturally occurring and have the potential to be biocompatible. These polypeptides can also adopt secondary structures to further improve the stability of the vesicles. Our laboratory previously investigated the novel poly(L-glutamate)$_{60}$-*b*-poly(L-leucine)$_{20}$ ($E_{60}L_{20}$) block copolypeptide synthesized by the laboratory of Timothy Deming. In this polypeptide, the hydrophilic glutamate segment assumes a random coil while the hydrophobic leucine segment forms an alpha helix. The $E_{60}L_{20}$ block copolypeptide therefore has a truncated cone shape that favors self-assembly into vesicles (EL vesicles). The size of the EL vesicles could be controlled by serial extrusion, and the EL vesicles were not cytotoxic to cells. Additionally, when previously conjugated with transferrin (Tf), a widely used cancer targeting ligand, the EL vesicles exhibited increased cellular uptake. These characteristics suggested that the EL vesicle could be used as a potential drug delivery vehicle.

This thesis extended our investigation of these vesicles, specifically, the thesis focused on the ability of the EL vesicle to encapsulate and deliver doxorubicin (DOX), a commonly used chemotherapeutic. Polyethylene glycol (PEG) was conjugated to the EL vesicles to maintain

vesicle stability during the drug loading process and for providing stability in the future for *in vivo* applications. DOX was successfully encapsulated while maintaining stable EL vesicles using a modified pH-ammonium sulfate gradient method. Tf was then conjugated to the drug-loaded EL vesicles to create a stable, targeted drug delivery vehicle. A mathematical model was developed to predict drug release from the targeted, drug-loaded EL vesicles by considering the transient diffusion of DOX across the vesicle bilayer and the time-dependent mass balances on DOX in the interior core and exterior aqueous solution. Release profiles were predicted by applying the method of lines approach with an ordinary differential equation solver in MATLAB. *In vitro* release experiments were performed to confirm the predicted release profiles, and the DOX diffusion coefficient in the vesicle bilayer was estimated. An *in vitro* cytotoxicity assay was subsequently performed with a cancer cell line with both the targeted and non-targeted, drug-loaded EL vesicles. The targeted, drug-loaded EL vesicles demonstrated an improved drug delivery efficacy compared to the non-targeted, drug-loaded EL vesicles.

The thesis of Brian Sangwoo Lee is approved.

Timothy J. Deming

Yi Tang

Daniel T. Kamei, Committee Chair

University of California, Los Angeles

2014

Dedicated to my mother and God.

Table of Contents

ACKNOWLEDGMENTS

First, I thank God for blessing me with such supportive people throughout my incredible experience at UCLA. I would not have been able to complete this journey without them. I would like to sincerely thank Dr. Daniel T. Kamei who has been my mentor for the past three years. Dr. Kamei is so passionate about making everyone, including myself, into better researchers and better people. Dr. Kamei has always preached how important it is to be a man of character who respects others and remains true to one's self in the face of adversity. I respect how he was never afraid to let me know when I had made a mistake and told me how I could improve. Dr. Kamei has also been a father figure who has believed in me. I know that there were many times, especially this past year, when I stressed him, but he remained patient with me. He always offered to listen to my concerns and shared both my joys and my struggles. Very rarely will you find someone who is so invested in his or her students, and I truly appreciate everything he has done for me. On a lighter note, I will miss his spot-on sports analogies on how to tackle research. They make perfect sense every time!

Growing with the entire Kameizing Lab family has also made my journey such a rewarding experience. I would like to thank my graduate student, Mike Choe, for teaching me everything I know about the vesicle project. His positive attitude and laughter were contagious, and I will never forget the time we won our first "Kamei Lab Games" together. Ricky Chiu and Kristine Mayle have been great mentors by constantly providing feedback on experiments and sharing their enthusiasm for research. Garrett Mosley and David Pereira, my fellow Maroon 3 members, were great company in the student offices. Also, I want to thank the most recent graduate student, Sherine Cheung, and the previous graduate students, Foad Mashayekhi, Dennis Yoon, and Tracy Ying, for being a part of my Kamei Lab experience. Allison Yip and Alison

Thach have been the best undergraduate researchers that anyone could ask to work with. They were always willing to assist me with the vesicle experiments and have made many contributions for the vesicle project's success. My co-members Bob Lamm, Cameron Yamanishi, and Johnny Wang have been some of my closest friends during our years together. And thanks to all the previous and current undergraduate researchers, Will, Kevin, Gretchen, Alec, Christina, Devin, Parsa, Stephanie, Erik, Phuong, Katie, Sam C., Sam Z., Kevin, and Amy, for the awesome memories we have made.

I would like to also thank Dr. Timothy J. Deming for providing guidance on the vesicle project. It has been a pleasure collaborating with him and his lab on this fascinating project.

Finally, I would like to thank my friends and family for always supporting me, especially my mother, Nina. She has been my role-model as her strong will and perseverance have inspired me to never give up in the face of adversity. She has encouraged me daily with phone calls and messages, and I will never forget the sacrifices she has made so that I could pursue my goals.

Figure 2.1 was reprinted from Barenholz with permission from Elsevier.

1. Motivation and Background

1.1. Cancer

According to the American Cancer Society, cancer is the second leading cause of death in the United States. In 2014, 1,665,540 new cancer cases are projected along with 585,720 cancer deaths [1]. Cancer remains the leading cause of death among the 20 year age group of adults between 40 and 79 years-old. Furthermore, it is the first or second leading cause of death among every 20 year age group for females. Lung and bronchus, prostate, and colorectum cancer account for approximately half of cancer deaths among men, while lung and bronchus, breast, and colorectum cancer account for more than a quarter of cancer deaths among women [1].

Surgical resection of tumors has remained as one of the most effective treatments for localized tumors [2]. As a result of improvements in surgery over the past two decades, the mortality rate associated with patients who have undergone surgery for tumors has been reduced significantly [2]. However, one limitation of surgery is that it remains ineffective in treating metastatic tumors. In some cases, surgery may be able to treat confined metastatic tumors, but this only represents 10-15% of cancer cases [3].

Radioation therapy, which uses ionizing radiation to kill cancer cells, is an alternative treatment option for cancer. The most common method of administering radiation therapy is external beam radiation where high-energy rays are directed to the tumor location and non-invasively delivered from outside of the body. This has become an increasingly popular treatment method as approximately 50% of all cancer patients will receive some form of radiation therapy, either as the sole method of treatment or in combination with surgery [4]. Furthermore, radiation therapy has had success with a 40% cancer cure rate [5]. However, radiation therapy can lead to local side effects in the tissue or organs that have been irradiated

due to the death of normal, healthy cells. Short term effects include skin erythema, nausea, and diarrhea, and long term effects include radiation-induced fibrosis, vascular damage, and neural damage [6].

Another treatment option is chemotherapy, which is the delivery of small molecule drugs to kill the rapidly proliferating cancer cells. Unlike surgery and external beam radiation, which are local treatments, chemotherapy is a systemic treatment, where the drug travels throughout the body and eventually reaches the cancer cells. One of the most commonly used chemotherapeutics for multiple cancers is doxorubicin (DOX). DOX is an anthracycline that kills the cell by intercalating with DNA, thus disrupting topoisomerase-II-mediated DNA repair, and by generating free radicals that damage the cell's DNA and proteins [7]. However, one issue with the naked delivery of DOX is its nonspecificity, since it can affect both cancer and healthy cells. This can result in the death of normal rapidly proliferating cells, such as, blood cells in the bone marrow, hair follicles, and the digestive tract, which can result in low blood cell count, hair loss, and nausea and vomiting, respectively. Furthermore, DOX administration has also been found to cause cardiotoxicity [8]. These side effects have limited the adminstered dosage of DOX. This can result in failure of the therapy and possibly lead to further metastatic tumors. To circumvent this problem, researchers have been exploring methods to deliver the drug specifically to cancer cells to reduce the damage to healthy cells.

1.2. Drug Delivery Vehicles

An ideal solution to overcome the limitations of the naked delivery of chemotherapeutics is to encapsulate the chemotherapeutic within a nano-sized drug delivery vehicle. Nano-sized drug delivery vehicles are advantageous since they can protect the drug from degradation during its circulation in the body, release the drug in a controlled manner, and provide passive targeting

to the tumor tissue through the enhanced permeability and retention (EPR) effect [9], [10]. A wide variety of carriers such as nanoparticles have been investigated for drug delivery purposes. For this introduction, we will focus on some of the work performed with self-assembled drug delivery vehicles including liposomes, polymersomes, and polypeptide hybrid vesicles.

Among these drug carriers, liposomes, which are vesicles composed of natural or synthetic phospholipids, have been the most studied [11]. As a result, many liposomal formulations have been approved for cancer treatments, and many are currently undergoing clinical trials [12]. One example of a successful, FDA-approved liposomal formulation is Doxil, which is now used to treat recurrent ovarian cancer, breast cancer, and multiple myeloma [13]. Doxil is a DOX-loaded liposome composed of hydrogenated soybean phosphatidylcholine, cholesterol, and 1,2-distearoyl-sn-glycero-3-phosphoethanolamine conjugated with polyethylene glycol-2000 (PEG_{2000}) [12]. The benefits of encapsulating DOX within a liposome carrier were demonstrated in a Phase III clinical trial of Doxil where Doxil exhibited reduced cardiotoxicity and fewer incidents of neutropenia and vomiting compared to free DOX [12]. Doxil also performed better than other DOX-liposome systems due to the presence of PEG. PEG is a highly soluble polymer that provides steric stabilization by decreasing liposome-liposome aggregation, preventing adsorption of serum proteins, and decreasing uptake by macrophages [14]. This resulted in Doxil having a significantly greater elimination half-life of 41-70 hours compared to 2-3 hours of DOX-loaded liposomes [12].

While liposome systems have been successful in the market, one limitation of liposomes is that PEG is often required to improve the liposome's *in vivo* stability. This is undesirable as high densities of PEG on the lipids can result in larger hydrophilic PEG heads, leading to the formation of micelles due to the conical shape of the resulting molecule [15]. To counter this, the

hydrophobic chain must be increased, which is not possible with phospholipids. This has motivated the use of synthetic polymers, which also self-assemble to form stable and biocompatible vesicles called polymersomes. Unlike phospholipids, synthetic control of the polymers allows for tunability of the hydrophilic to hydrophobic chain lengths [15]. Although polymersomes are still in the research phase, polymersomes have seen success in drug delivery. With regards to pharmacokinetics, Discher and coworkers prepared PEG-*block*-poly(ethylethylene) and PEG-*block*-poly(butadiene) copolymers that formed stable polymersomes with *in vivo* circulation half-lives exceeding that of PEG-coated liposomes [16]. For drug delivery, the Discher group also successfully encapsulated DOX and paclitaxel (TAX) within PEG-(polylactic acid) (PLA) and PEG-(polycaprolactone) (PCL) polymersomes. When administered in an *in vivo* experiment, the (DOX+TAX)-loaded polymersomes exhibited a two-fold increase in cell death of mice tumors compared to free drugs, and a single injection of the polymersomes shrunk mice tumors by 50% within 5 days [17].

In addition to polymers, polypeptide hybrid molecules have been rising in popularity as materials for drug delivery systems. A polypeptide hybrid polymer corresponds to a macromolecule comprised of a polypeptide and another type of polymer. The polypeptide hybrid molecules introduce additional characteristics such as functional groups for conjugation, decreased toxicity, biodegradability, and the formation of secondary structures [18]. Similar to polymersomes, vesicles assembled with polypeptide hybrid polymers have been successful in encapsulating chemotherapeutics for drug delivery. Zhang and coworkers encapsulated DOX within novel amphiphilic [poly(ε-benzyloxycarbonyl-L-lysine)]$_2$-*block*-poly(ethylene glycol)-*block*-[poly(ε-benzyloxycarbonyl-L-lysine)]$_2$ (PzLL$_2$-PEG-PzLL$_2$) vesicles [19]. Through confocal laser scanning microscopy, they observed that the DOX-loaded PzLL$_2$-PEG-PzLL$_2$

vesicles were internalized into MCF-7 cells and that the DOX was released within the cells and diffused towards the nuclei [19].

Both polymers and polypeptide hybrid polymers have shown many benefits over phospholipids. These biocompatible materials provide greater synthetic control to tailor the polymer for a desired application and functionality for further chemical modification. Additionally, polymersomes are stable structures for drug delivery, and they are able to load and effectively deliver drugs. Although the investigation of polymers and polypeptide hybrid polymers for drug delivery is relatively new compared to phospholipids, they have the potential to become materials that can be used to form drug delivery vehicles in future cancer treatments.

1.3. Previous Work with Block Copolypeptides

Previous members of the Kamei Lab have investigated multiple block copolypeptides synthesized by the Deming Lab for applications in drug delivery. A poly(L-lysine)$_{60}$-*b*-poly(L-leucine)$_{20}$ ($K_{60}L_{20}$) block copolypeptide was previously reported to self-assemble into vesicles, which could be manipulated to different sizes and also encapsulate hydrophilic cargo [20]. In order to better understand the formation of $K_{60}L_{20}$ vesicles, the effects of altering the hydrophilic-hydrophobic ratio of the block copolypeptide were investigated by tuning the length of the hydrophobic segment while keeping the hydrophilic segment constant. In these studies, the $K_{60}L_{10}$, $K_{60}L_{15}$, $K_{60}L_{20}$, and $K_{60}L_{25}$ block copolypeptides were synthesized and investigated [21].

All of the KL polypeptides were observed to form vesicles. However, the $K_{60}L_{10}$ block copolypeptides gave rise to many more micelles in the population of self-assembled supermolecular structures [21]. This was consistent with the fact that the $K_{60}L_{10}$ molecule assumes a conical shape due to the shortened, disordered hydrophobic segment, which leads to self-assembly into micelles [22]. In contrast, the longer hydrophobic segments form a truncated

cone molecular shape that favors the formation of vesicles, and fewer micelles were observed in this population. However, too long of a hydrophobic chain length was undesirable as it caused the vesicles to become too rigid to manipulate their sizes. Specifically, the $K_{60}L_{20}$ vesicles were monodisperse after serial extrusion, while the $K_{60}L_{25}$ vesicles were still fairly polydisperse after extrusion [21].

The effects of the hydrophobic chain length on cytotoxicity were also examined. The $K_{60}L_{10}$ suspensions were more cytotoxic than the $K_{60}L_{20}$ suspensions, most likely due to the micelles being more toxic than the vesicles [21]. When dialysis was performed to remove the micelles but retain the vesicles, the mass of the $K_{60}L_{10}$ block polypeptides decreased more than the mass of $K_{60}L_{20}$ block polypeptides, confirming that $K_{60}L_{10}$ had smaller aggregates that could be dialyzed away. However, the dialyzed $K_{60}L_{10}$ suspensions remained more toxic than the $K_{60}L_{20}$ suspensions even after dialysis, suggesting that the $K_{60}L_{10}$ vesicles were inherently unstable and led to smaller aggregates (when placed in media) that were toxic to cells. Ethanol treatment, an established method used to observe the stability of vesicles, was performed on the $K_{60}L_{10}$ and $K_{60}L_{20}$, and it was found to disrupt the vesicle structure of the $K_{60}L_{10}$ vesicles but not the $K_{60}L_{20}$ vesicles [21]. From this study, it was concluded that $K_{60}L_{20}$ was the optimal hydrophilic-hydrophobic ratio for the formation of stable vesicles, and this ratio was used for the development of future block copolypeptides for vesicle formation.

Since the $K_{60}L_{20}$ polypeptides consisted of cationic lysine groups, they were potential gene carriers that could complex with negatively charged DNA. However, initial uptake studies showed that the $K_{60}L_{20}$ vesicles were not able to enter cells. This was problematic since DNA must cross several barriers of the cell for successful transfection. Another cationic block copolypeptide, the poly(L-arginine)$_{60}$-*b*-poly(L-leucine)$_{20}$ ($R_{60}L_{20}$), was investigated for gene

delivery purposes. Previous studies have shown that arginine-rich peptides have the ability to cross the cell membrane due to a bidentate binding between the guanidinium group and the anions of the cell membrane [23], [24], [25]. Additionally, poly(L-arginine) homopolymers have been previously used to deliver plasmid DNA into cells [26]. Therefore, the $R_{60}L_{20}$ vesicles were suitable candidates as transfection agents.

Like the $K_{60}L_{20}$ polypeptides, the $R_{60}L_{20}$ polypeptides self-assembled into vesicles. Additionally, the $R_{60}L_{20}$ vesicles remained stable when complexed with the DsRed plasmid at a +/- charge ratio of 10:1, and the complex successfully transfected many HeLa cells [25]. However, the $R_{60}L_{20}$ vesicles transfected fewer cells than Lipofectamine 2000, which is a commercially available transfecting agent [25]. One possible explanation for the reduced transfection efficiency was the increased stability of the $R_{60}L_{20}$ vesicles with the negatively charged DNA since higher concentrations of heparin were required to dissociate the plasmid from the $R_{60}L_{20}$ vesicles than Lipofectamine 2000 [25]. While this may have reduced the transfection efficiency, this was also advantageous since the $R_{60}L_{20}$ vesicles induced a negligible immune response in RAW264.7 cells, as evidenced by lower interleukin-6 (IL-6) levels [25].

While the $R_{60}L_{20}$ vesicles showed promise as potential *in vivo* transfection agents, one limitation of these positively charged polypeptides was that they were toxic to cells at higher concentrations required for delivery of small molecule chemotherapeutic drugs. This has prevented the $R_{60}L_{20}$ vesicles from delivering chemotherapeutics such as doxorubicin (DOX), which require higher doses to exert their therapeutic effect, and therefore, require higher concentrations of vesicles to be administered [17]. An anionic poly(L-glutamate)$_{60}$-*b*-poly(L-leucine)$_{20}$ ($E_{60}L_{20}$) block copolypeptide was previously reported. Similar to the $K_{60}L_{20}$ and $R_{60}L_{20}$ block copolypeptides, the $E_{60}L_{20}$ block copolypeptides also self-assemble into spherical

vesicles (EL vesicles) that could be controlled in size and that could encapsulate hydrophilic cargo [20]. More importantly, the EL vesicles were less cytotoxic to cells since they were negatively charged and could not interact with the net negatively charged cell membrane [27]. However, a limitation of the EL vesicles was their inability to enter cells on their own, which has prevented their delivery of therapeutics with intracellular targets.

To overcome this challenge, transferrin (Tf), a widely used cancer targeting ligand, was conjugated to the EL vesicles. Tf is a 78 kDa iron-binding glycoprotein whose main function is to bind to and transport iron, a nutrient for cellular proliferation, throughout the body [28]. To deliver iron to the cell, Tf binds to the transferrin receptor (TfR), after which it is internalized by clathrin-mediated endocytosis [29]. Since cancer cells require more iron to sustain their rapid proliferation, cancer cells overexpress TfR on their surface, and Tf has become widely used as a cancer-targeting agent [29].

Tf was successfully conjugated to fluorescein isothiocyanate (FITC) labeled EL vesicles to create Tf-conjugated EL (Tf-EL) vesicles. The Tf-EL vesicle was not cytotoxic to cells, which was predictable since neither Tf nor the EL vesicles were toxic individually. The cellular uptake was then monitored in LAPC-4 and PSCA-transfected 22Rv1 cells. For both cell lines, the FITC-labeled EL vesicles had a low level of fluorescence in the cells due to minimal uptake [27]. However, the Tf-EL vesicles showed an enhanced cellular uptake with much greater levels of fluorescence inside the cells. The mechanism of internalization was then determined by treating the cells with drugs that inhibited different pathways including macropinocytosis, clathrin-mediated endocytosis, and caveolae-mediated endocytosis. The caveolae-mediated endocytosis inhibitors resulted in minimal inhibition of Tf-EL vesicle internalization. The macropinocytosis inhibitors led to some inhibition, and the inhibitors of clathrin-mediated endocytosis resulted in

the greatest level of inhibition. Thus, clathrin-mediated endocytosis was the dominant pathway for endocytosis for the Tf-EL vesicles, and macropincotysosis played a minor role in their uptake behavior. This suggested that the Tf molecules on the vesicles binding to the Tf receptors on the cells was primarily responsible for the internalization since the Tf ligand itself enters cells via clathrin-mediated endocytosis.

After determining the internalization pathway, the destination of the internalized Tf-EL vesicles was determined by immunostaining for the early endosome antigen-1 (EEA-1) and the lysosomal-associated membrane protein-1 (LAMP-1). The Tf-EL vesicle was fluorescently labeled green, while the secondary antibody for the primary antibody for EEA-1 and LAMP-1 was fluorescently labeled red. In such an experiment, yellow and orange fluorescence corresponded to the vesicle being colocalized with either the early endosome or lysosome. Colocalization was not observed for the antibody for LAMP-1 for all conditions tested, while colocalization was observed when using the EEA-1 antibody. These results suggested that the Tf-EL vesicles did not traffic to the lysosome, but rather entered the early endosome and quickly recycled back to the cell surface. This was consistent with the trafficking pathway of other molecules that enter cells by clathrin-mediated endocytosis and macropinocytosis. Despite the rapid recycling by the early endosome, other drug delivery vehicles conjugated with Tf have reported improved drug delivery efficacies [30].

In this thesis, we will discuss the EL vesicle's performance as a drug delivery vehicle. Chapter 2 summarizes the formation and characterization of the targeted drug delivery system, specifically, the transferrin-conjugated, DOX-loaded and PEGylated EL (Tf-DPEL) vesicles. In Chapter 3, we predict the drug release from the Tf-DPEL vesicles using a mathematical model,

which was then confirmed with drug release experiments. Chapter 4 investigates the drug delivery efficacy of the Tf-DPEL vesicles compared to the non-targeted DPEL vesicles.

2. Drug Encapsulation to Develop a Targeted, Drug-Loaded EL Vesicle

2.1. Motivation and Background

Doxorubicin (DOX) is a widely used chemotherapeutic to treat various cancers. Encapsulation of DOX has been an effective way to protect the drug while it is in the bloodstream and to minimize the nonspecific toxic effects on healthy cells. DOX is commercially available as doxorubicin hydrochloride, and it is a weak amphipathic base (pKa = 8.3), mainly due to the primary amine group, which can primarily exist as protonated or deprotonated according to the Henderson-Hasselbalch equation. Thus, DOX can exhibit either hydrophilic or hydrophobic properties by adjusting the environmental pH. Researchers have taken advantage of this tunable property of DOX to develop various drug loading strategies. These drug loading methods, including the physical entrapment of DOX and loading by a transmembrane gradient, have been successful in vesicles.

Physical entrapment of DOX during vesicle formation is a simple drug loading method. To encapsulate DOX during vesicle processing, the amphipathic building blocks of the vesicles and DOX are first dissolved in an organic solvent such as DMSO. An aqueous solution buffered to a basic pH is then added to the organic solvent. The basic pH ensures that DOX exists in its deprotonated form and is hydrophobic. As the aqueous solution is added, the hydrophobic tails of the building blocks and the DMSO assemble into a hydrophobic bilayer due to hydrophobic interactions. The deprotonated DOX is also driven to this hydrophobic bilayer due to the same hydrophobic effect. Meanwhile, the hydrophilic heads maximize their interactions with the aqueous solution, thus forming vesicles with DOX encapsulated in the hydrophobic bilayer.

An alternative DOX loading method that can be performed after the vesicles have been formed is remote loading via a transmembrane pH gradient. In this method, the vesicles are first

prepared by dissolving the building blocks in an organic solvent followed by the addition of an acidic buffer. The newly formed vesicles then contain an acidic aqueous core, while the exterior buffer can be titrated to a basic pH. DOX is then added to the exterior buffer such that it is deprotonated and in its neutral form. In this form, DOX exhibits hydrophobic properties that allow it to enter and diffuse across the vesicle bilayer. Upon exposure to the aqueous core, DOX is protonated by the acidic environment and is trapped within the vesicle [31], [32].

Researchers have also employed the ammonium sulfate gradient, as it provides the additional advantage of vesicle stability. In this method, the following gradient must be created such that $[(NH_4)_2SO_4]_{lip} \gg [(NH_4)_2SO_4]_{med}$ (Figure 2.1), where $[(NH_4)_2SO_4]_{lip}$ and $[(NH_4)_2SO_4]_{med}$ are the intraliposomal and external ammonium sulfate concentrations, respectively [13]. Preparing this gradient is very similar to the protocol used for the pH gradient method. First, the building blocks are dissolved in an organic solvent followed by addition of ammonium sulfate, resulting in vesicles with ammonium sulfate in the aqueous core. The $(NH_4)_2SO_{4,med}$ can then be exchanged using dialysis or column chromatography for a buffer that does not contain ammonium sulfate but contains other salt ions corresponding to the same osmotic pressure. DOX is then added to the external environment, where it can be deprotonated (but not to a significant extent), pass through the hydrophobic bilayer, and enter the aqueous core. DOX is then reprotonated by an acidic aqueous core that is established by $(NH_4)_2SO_{4,lip}$. Although an acidic buffer is not used in this protocol, an acidic environment is generated as $(NH_4)_2SO_{4,lip}$ dissociates to SO_4^{2-} and NH_4^+, which further dissociates into NH_3 and H^+ ions [33]. The newly formed H^+ ions protonate the incoming DOX, and the interior proton pool is maintained as neutral ammonia leaves the intraliposomal environment, driving the dissociation of the remaining ammonium sulfate [33].

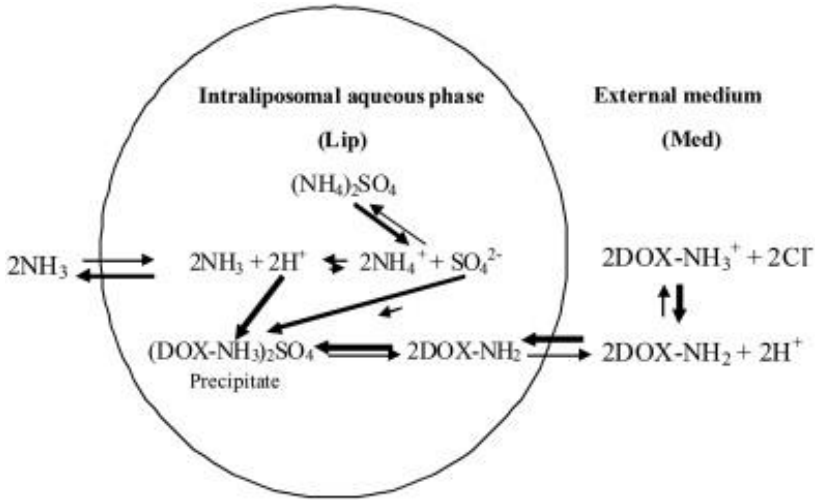

Figure 2.1: A schematic showing the mechanism in which DOX is loaded into liposomes using the ammonium sulfate gradient method. $(NH_4)_2SO_4$, initially present inside the liposome (Lip), dissociates into $2NH_4^+$ and SO_4^- ions. NH_4^+ gets deprotonated and released from the liposome while SO_4^- remains. When DOX is introduced into the external medium (Med), some of the DOX molecules become deprotonated and cross the liposome bilayer. Upon entering the aqueous phase, the DOX molecules are reprotonated and then can interact with SO_4^- to create an insoluble DOX_2SO_4 complex. Reprinted from Barenholz [13] with permission from Elsevier.

The ammonium sulfate gradient provides an additional benefit by stabilizing the vesicles during drug loading. After DOX is reprotonated in the aqueous core, the protonated DOX can interact with SO_4^{2-} to create a DOX_2SO_4 complex. The solubility of this DOX_2SO_4 complex is less than 2 mM, causing it to precipitate out of solution at high concentrations [13]. Using cryo-electron microscopy, Lasic and coworkers have shown that the DOX_2SO_4 complex precipitate exhibits a fiber-like gel structure [34]. This acts to minimize the intraliposomal osmotic pressure exerted on the vesicles to stabilize the drug loading process.

When the 3 above mentioned methods were applied to load DOX within the EL vesicles, they resulted in either unstable vesicles or unsuccessful encapsulation. The physical entrapment method created a polydisperse population of EL vesicles that could not be extruded to create monodisperse vesicles. Similarly, the pH gradient method resulted in aggregation of the EL

vesicles. While the ammonium sulfate gradient did not result in any aggregation, the amount of loaded DOX was minimal. Therefore, in order to improve drug loading with the ammonium sulfate gradient method, we combined features from the pH gradient method with the ammonium sulfate gradient method.

It has been reported that the role of the ammonium sulfate is mainly for loading stability rather than drug loading itself [35]. Although the ammonium sulfate assists in drug loading by inducing acidification of the aqueous core and creating a pH gradient, the exterior pH remains unaffected, preventing efficient DOX loading. We therefore investigated establishing an ammonium sulfate gradient, followed by exchanging the outside solution with a buffer of pH greater than 8.3 to further deprotonate DOX and drive greater amounts of DOX into the aqueous core.

In this chapter, we summarize our work in modifying the EL vesicles to convert it into a targeted drug delivery vesicle. The size, stability, and DOX loading content were characterized as the EL vesicles were extruded, conjugated with polyethylene glycol (PEG), DOX loaded, and conjugated with transferrin (Tf) in order to create a transferrin-conjugated, DOX-loaded, and PEGylated EL (Tf-DPEL) vesicle.

2.2. Materials and Methods

2.2.1. Materials

$E_{60}L_{20}$ block copolypeptides were generously provided by the Deming Lab at UCLA. The Bradford reagent was obtained from Bio-Rad (Hercules, California). Dialysis bags (MWCO = 8,000 Da) were purchased from Spectrum Laboratories (Rancho Dominguez, California). The 1000 nm, 400 nm, and 200 nm polycarbonate membranes were purchased from Whatman Nuclepore (Florham Park, New Jersey). The Avanti Mini-Extruder was purchased from Avanti

Polar Lipids Inc. (Alabaster, Alabama). Zeba desalt spin columns, N-hydroxysuccinimide (NHS), and 1-ethyl-3-(3-dimethylaminopropyl) carbodiimide (EDC) were purchased from Pierce (Rockford, Illinois). The poly(ethylene glycol)$_{5000}$ to conjugate onto the vesicles were purchased from Nanocs (New York, New York). Spin concentrators (MWCO = 100,000 Da) were purchased from Millipore (Billerica, California). All other reagents, such as apo-transferrin (apo-Tf), were purchased from Sigma-Aldrich (St. Louis, Missouri) unless otherwise noted.

2.2.2. Processing the EL Vesicles

The $E_{60}L_{20}$ block copolypeptide was synthesized by the Deming Lab using the transition metal-mediated α-amino acid *N*-carboxyanhydride (NCA) polymerization technique [36]. A solution of 0.5% w/v polypeptide in tetrahydrofuran (THF) was first prepared. This solution was sonicated for 30 minutes, followed by a 30 minute interval of inactivity, and then another 30 minutes of sonication to ensure dissolution of the polypeptide. Subsequently, filtered water was added drop wise to the solution while vortexing such that the final suspension was a 2:1 volume ratio of THF to water. This resulted in a vesicle concentration of 0.333% w/v. In order to remove the remaining THF, the resulting suspension was dialyzed (MWCO = 8,000 Da) against filtered water overnight with water bath changes every hour for the first 3 hours. After dialysis, the final EL vesicle concentration was set to 0.2% w/v with filtered water.

2.2.3. Extrusion of EL Vesicles

To prepare the processed vesicles for future subsequent drug loading procedures, the appropriate amount of a 50 μM of ammonium sulfate solution was added such that the final suspension had an ammonium sulfate concentration of 5 μM. The vesicles were then serially extruded through 1000 nm, 400 nm, and 200 nm Whatman Nuclepore polycarbonate membranes using the Avanti Mini-Extruder. The size and polydispersity index (PdI) were measured using

the Malvern Zetasizer Nano ZS model Zen 3600 (Malvern Instruments Inc., Westborough, Massachusetts). The Bradford assay was performed to quantify the final concentration of vesicles by using the post-dialyzed vesicles as the standard.

2.2.4. Conjugating Polyethylene Glycol (PEG)

PEG was conjugated onto the vesicles using EDC/NHS chemistry to activate the carboxylate groups on the EL vesicle surface. A 25,000-fold excess of EDC and NHS were added to the vesicles, and the mixture was incubated with the vesicles together for 25 minutes. A 0.5 M phosphate buffer (PB) solution was then added to raise the pH of the suspension to 7.0 and quench the reaction. Subsequently, a solution was added such that the 12,500-fold ratio of methoxy-poly(ethylene glycol)$_{5000}$-amine (mPEG):vesicle and 12,500-fold ratio orthopyridyl disulfide-poly(ethylene glycol)$_{5000}$-amine (biPEG):vesicle molar ratios were added both 12,500:1. This mixture was incubated together for 2 hours. Methoxy-poly(ethylene glycol)$_{5000}$-amine (mPEG), is amine functionalized on one end whereas the orthopyridyl disulfide-poly(ethylene glycol)$_{5000}$-amine PEG (biPEG) is amine functionalized on one end and functionalized with an orthopyridyl disulfide (OPSS) group on the other end. The sample was purified using a spin concentration filter (MWCO = 10,000 Da) and suspended in 500 µL of 1x Tris buffer. The sample size and PdI were measured using dynamic light scattering.

2.2.5. Encapsulating Doxorubicin

A 4:10 mass ratio of DOX to EL vesicles was calculated. This amount of DOX was then aliquoted and placed in a separate tube. The DOX and vesicle sample were then separately heated at 65˚C in a water bath for 2 minutes. The DOX was then added to the suspension of PEGylated vesicles in 50 mM Tris buffer and placed in a 65˚C water bath for 1 hour. The DOX-

loaded vesicles were then purified from free DOX using a spin concentrator (MWCO = 10,000 Da).

2.2.6. Conjugating Transferrin (Tf)

Prior to conjugating Tf, apo-Tf was iron loaded to make holo-Tf. Briefly, 20 µL of the iron chelating agent nitrilotriacetate (NTA) was mixed with 10 µL of 250 mM iron (III) chloride. A 10 mg/mL solution of apo-Tf in a 50 mM 4-(2-hydroxyethyl)-1-piperazineethanesulfonic acid (HEPES) buffer containing 20 mM sodium bicarbonate was also prepared. The chelated iron was then added to the apo-Tf solution and allowed to iron load overnight at room temperature. The following day the holo-Tf (iron-loaded Tf) was purified from the free iron using a Zeba desalt spin column and then thiolated for an hour using Traut's reagent. Afterward, the thiolated Tf was purified with a Zeba desalt spin column. The thiolated Tf was then added to the DOX loaded and PEGylated, EL vesicle and allowed to react overnight with constant mixing. In order to purify free Tf from the Tf-DPEL vesicles, size exclusion chromatography was performed. A column was packed with Sepharose CL-4B beads and rinsed with 12 mL of the HEPES elution buffer. This column was then stored in a 4˚C refrigerator until use. After the Tf conjugation, the concentrated sample was added into the column. Fractions were taken every two minutes while running more of the HEPES bicarbonate elution buffer through the column. The first fraction that was red was collected and verified by DLS to contain the desired Tf-DPEL population.

2.2.7. Determining the Tf-DPEL Vesicle DOX Concentration

Following purification, the concentration of DOX within the Tf-DPEL vesicle population was determined using a UV-visible Spectrophotometer. 20 µL of the Tf-DPEL vesicle sample was dissolved in 180 µL of DMSO for 1 hour. The absorbance of the mixture containing Tf-DPEL vesicles and DMSO was measured at 490 nm and 700 nm wavelengths using DMSO as

the blanking solution. The absorbance at 490 nm was subtracted by the absorbance at 700 nm (the background absorbance) and then compared to a standard curve with known DOX concentrations. The encapsulation efficiency was then calculated:

$$Encapsulation\ efficiency\ = \frac{\mu g\ of\ DOX\ encapsulated\ in\ vesicles}{\mu g\ of\ initial\ DOX\ added} \tag{2.1}$$

The loading ratio was also determined:

$$Loading\ ratio\ = \frac{\mu g\ of\ DOX\ encapsulated\ in\ vesicles}{mg\ of\ initial\ polypeptide} \tag{2.2}$$

2.3. Results and Discussion

2.3.1. Characterization of the Tf-DPEL Vesicles

The size and stability of the Tf-DPEL vesicles were evaluated with dynamic light scattering and DIC imaging. The EL vesicles were polydisperse after processing and in the micron size range (DIC images not shown). By extruding the vesicles through 200 nm polycarbonate filters in the presence of a buffered ammonium sulfate solution, we were able to generate a fairly monodisperse population of vesicles with a diameter of 179 nm (Table 2.1). Since glutamate residues were readily present on the surfaces of the EL vesicles, EDC/NHS chemistry was used to conjugate PEG to the EL vesicles where 25,000 PEG molecules per vesicle were added. PEG provided steric stability during the DOX loading process and also has the potential to provide *in vivo* stability. For the non-targeted DPEL vesicles, only methoxy-poly(ethylene glycol)$_{5000}$-amine (mPEG) was added. For the Tf-DPEL vesicles, orthopyridyl disulfide-poly(ethylene glycol)$_{5000}$-amine (biPEG) and mPEG were added in a 1:1 ratio such that 12,500 mPEG per vesicle and 12,500 biPEG per vesicle were added. The biPEG acted as a linker for the attachment of Tf to create the Tf-DPEL vesicles. One side of the biPEG contained an

amine group to attach to the glutamate residues of the vesicles, and the other end corresponded to an orthopyridyl disulfide (OPSS) group that allowed the formation of disulfide bonds with the thiolated Tf. The addition of PEG to create PEGylated EL vesicles (PEL) decreased the diameter to 173 nm (Table 2.1). Since the vesicles are self-assembled structures, their size can change as they are modified.

Table 2.1: The size and polydispersity index (PdI) of the vesicles as they are modified to create the Tf-DPEL vesicles. The encapsulation efficiency and loading content were only measured for the Tf-DPEL vesicles since only the Tf-DPEL vesicles contained drug.

Table 2.1				
Conjugation Step	**Diameter (nm)**	**Polydispersity Index (PdI)**	**Loading Content (%)**	**Encapsulation Efficiency (%)**
Extruded EL Vesicle	179 ± 3.70	0.170 ± 0.024	-	-
PEL Vesicle	173 ± 1.72	0.198 ± 0.006	-	-
Tf-DPEL Vesicle	152 ± 28	0.190 ± 0.001	15.3 ± 4.0	4.00 ± 0.05

DOX was then encapsulated within the vesicles using a modified pH-ammonium sulfate gradient to create DOX-loaded PEL vesicles (DPEL). Finally, 10,000 Tf molecules per vesicle were added to the biPEG linkers to provide active targeting towards cancer cells and a method for vesicle cellular uptake. Tf conjugation to create Tf-conjugated DPEL vesicles (Tf-DPEL) resulted in a diameter of 152 nm after size-exclusion chromatography purification (Table 2.1). By simply controlling the initial size of the extruded EL vesicles, we have been able to consistently obtain Tf-DPEL vesicles below 200 nm.

The diameter of the final Tf-DPEL vesicle construct satisfied the dual criteria for the ideal size of a drug delivery vehicle. Firstly, the diameter was within the 60 to 400 nm range, indicating that it could take advantage of the enhanced permeability and retention (EPR) effect [37]. The EPR effect allows the nano-sized drug carriers to preferentially accumulate into tumor tissues due to the abnormal characteristics of the tumor tissue, specifically, increased vascular

permeability and poor lymphatic drainage. The carrier can therefore reach high concentrations in the tumor compared to that in the plasma, thereby delivering the drugs preferentially to the cancer cells [10]. Secondly, the diameter of the Tf-DPEL vesicles was below 200 nm, which enabled the vesicles to be internalized via clathrin-mediated endocytosis [38].

Vesicle stability was assessed using the polydispersity index (PdI). The PdI values of the EL, PEL, and Tf-DPEL vesicles were 0.170, 0.198, and 0.190, respectively (Table 2.1). All PdI values were within the generally accepted range of 0 to 0.300 for a fairly monodisperse population. Despite undergoing multiple purification and conjugation steps, the vesicles maintained their overall integrity, possibly due to the intrinsic stability of polypeptide-based vehicles. The $E_{60}L_{20}$ block copolypeptides are larger building blocks compared to lipids, and therefore, experience greater van der Waals interactions to stabilize the vesicle structure. This allows for greater versatility of the EL vesicles as they can be modified post-synthesis whereas liposomes often require PEG modification prior to liposome formation.

2.3.2. DOX Encapsulation Using a Modified pH-Ammonium Sulfate Gradient

DOX was successfully encapsulated within the Tf-DPEL vesicles using a modified pH-ammonium sulfate gradient method. First, 0.5 M ammonium sulfate buffered to pH 5.48 was encapsulated during the extrusion process of the EL vesicles such that the final ammonium sulfate concentration was 0.05 M. This established an interior proton pool for the protonation of DOX as well as the ammonium sulfate for the formation of the DOX solid fibers. The exterior solution was buffered to pH 9 using Tris buffer to create the transmembrane pH-gradient so that DOX, originally present as doxorubicin hydrochloride, was deprotonated to its neutral form to more readily enter the vesicle core. The DOX loading procedure was performed at 65°C for 1 hr since previous reports state that increasing the incubation temperature of the drug above the

phase transition temperature of a lipid bilayer increases the bilayer permeability to promote drug loading and improve the loading efficiency [39]. Using this modified transmembrane gradient, DOX was successfully encapsulated within the Tf-DPEL vesicles, achieving an encapsulation efficiency of 4.00% (Table 2.1). This low encapsulation efficiency can be attributed to DOX being loaded into micelles and other aggregates that are present after the EL vesicles are processed. When we performed size exclusion column chromatography to purify the unconjugated Tf, we observed that a red color remained in the column after collecting our Tf-DPEL vesicle fractions, suggesting that DOX was loaded within the smaller micelles and aggregates. Since DOX was loaded into these undesirable structures, we obtained a low encapsulation efficiency for the Tf-DPEL vesicles. To better represent the DOX loaded in the Tf-DPEL vesicles, we also calculated the loading content, which is the mass of drug encapsulated divided by the mass of polypeptide used. We obtained a 15.3% loading content, which is comparable to other drug-loaded vesicle carriers systems reported in the literature.

3. Drug Release Profiles for the Tf-DPEL Vesicles

3.1. Motivation and Background

Drug encapsulation, in addition to protecting the drug from degradation, provides a measure of controlled release such that the drug is delivered at therapeutic doses upon reaching its target site and does not exhibit toxicity towards healthy tissue. In order to determine these release kinetics of the drug delivery vehicle, *in vitro* release studies must be performed. Furthermore, the *in vitro* release experiments can give insight into the *in vivo* performance of the system. Therefore, release studies are often prerequisites for *in vivo* experiments.

Mathematical modeling is an extremely useful approach to predict the release kinetics prior to performing any experiments. These models incorporate physical parameters, such as, the diffusion coefficient, size, and geometry of the vehicle [40]. Experimental drug release measurements can provide additional data to optimize the drug delivery system and guide future *in vitro* and *in vivo* cytotoxicity experiments. There are many models in the literature that have been used to describe drug release, most of which focus on the diffusion of drug across vehicles of many different geometries and properties [41].

The most commonly performed *in vitro* release experiment involves dialysis. Dialysis is a purification method that utilizes a dialysis tubing, which contains pores with a molecular weight cut off. This method is advantageous as it avoids the additional step of separating any free drug from the carrier [42]. This is achieved by selecting the dialysis tubing with a molecular weight cut off that is larger than the drug but smaller than the drug carrier. When this tubing is placed into a large water bath that acts as a sink, any drug that is released by the carrier will diffuse across the dialysis membrane into the sink compartment. Since the drug carrier is larger than the molecular weight cut off, it will remain in the dialysis tubing. Experimentally, one can either

measure the disappearance of drug from the carrier or the appearance of drug in the sink compartment [42].

In this chapter, we summarize the mathematical models that we developed to predict DOX release from the Tf-DPEL vesicles by considering transient diffusion through the vesicle bilayer and time-dependent mass balances on the moles of DOX in the interior and exterior aqueous compartments using the method of lines approach along with ordinary differential functions in MATLAB.

3.2 Materials and Methods

3.2.1. Materials

Dialysis bags (MWCO = 10,000 Da) were be purchased from Spectrum Laboratories (Rancho Dominguez, California). HEPES and sodium bicarbonate were purchased from Sigma-Aldrich (St. Louis, Missouri).

3.2.2. Mathematical Modeling of Drug Release

We developed a mathematical model to predict *in vitro* DOX release from the Tf-DPEL vesicles. Our model considered the unsteady-state diffusion of DOX across the vesicle bilayer. In diffusion, the molecules move due to random collisions and the transfer of thermal energy between molecules. Diffusional flux is mainly driven by a concentration gradient. Fick's Second Law, *i.e.*, a simplified form of the Conservation of Species equation for mass transfer, in spherical coordinates describes how the local membrane DOX concentration changes with time due to diffusional flux:

$$\frac{\partial C_{DOX,mem}}{\partial t} = D_{DOX}\left(\frac{\partial^2 C_{DOX,mem}}{\partial r^2} + \frac{2}{r}\frac{\partial C_{DOX,mem}}{\partial r}\right) \tag{3.1}$$

where $C_{DOX,mem}$ is the concentration of DOX in the membrane, t is time, and r is the radial distance from the center of the vesicle. D_{DOX} is the diffusion coefficient of DOX in the membrane, which is a physical parameter that describes the mobility of DOX in the Tf-DPEL vesicle membrane. For our model, D_{DOX} was assumed to remain constant throughout the entire Tf-DPEL vesicle bilayer. Additionally, it was assumed that DOX was dilute in the bilayer such that DOX only interacts with the membrane and not with other DOX molecules. In the differential equation, $C_{DOX,mem}$ depends on two independent variables, t and r. Therefore, it is a partial differential equation (PDE) where $\frac{\partial C_{DOX,mem}}{\partial t}$ is the first order partial derivative of $C_{DOX,mem}$ with respect to t, $\frac{\partial C_{DOX,mem}}{\partial r}$ is the first order partial derivative of $C_{DOX,mem}$ with respect to r, and $\frac{\partial^2 C_{DOX,mem}}{\partial r^2}$ is the second order partial derivative of $C_{DOX,mem}$ with respect to r.

Deriving an analytical solution for Eq. (3.1) would provide the exact mathematical solution for $C_{DOX,mem}$ as a function of t and r. However, analytical solutions are often difficult to derive even for simple models (Appendix 5.1). Alternatively, a solution can be determined numerically. Numerical solutions are advantageous since they can provide accurate estimations for complex equations, and they can be quickly calculated using a computer. We specifically employed the method of lines to numerically solve for the DOX concentration profile.

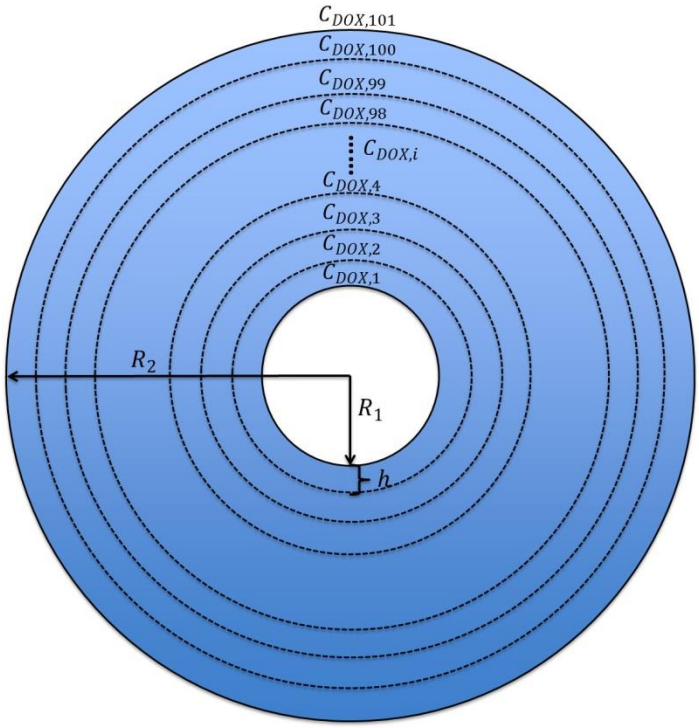

Figure 3.1: A schematic of the Tf-DPEL vesicle for applying the method of lines. The vesicle bilayer was divided into 101 nodes from R_1 to R_2 with a thickness h between nodes. Each node was also characterized by its own DOX concentration, $C_{DOX,i}$.

For the method of lines, the vesicle bilayer was first divided into a finite number of nodes as shown in Figure 3.1. The Tf-DPEL vesicle had an aqueous core radius of R_1 and a total radius of R_2. Since the accuracy of the solution increases with the number of nodes, we divided the Tf-DPEL vesicle membrane into 101 nodes. The nodes of the vesicle membrane were uniformly spaced by a thickness h:

$$h = \frac{R_2 - R_1}{100} \tag{3.2}$$

Every node was characterized by a drug concentration $C_{DOX,i}$, where i is an integer ranging from 1 to 101 that indexed a specific node. Therefore, the first node at R_1 was assigned a DOX

concentration $C_{DOX,1}$, and the second node positioned at $R_1 + h$ was assigned a DOX concentration $C_{DOX,2}$. This was repeated until node 101, which was positioned at $R_2 = R_1 + 100h$, with a DOX concentration $C_{DOX,101}$. Additionally, the non-boundary nodes, represented by $C_{DOX,i}$ for all i integer values excluding i=1 and $i = 101$, were each described by the PDE from Eq. (3.1):

$$\frac{\partial C_{DOX,i}}{\partial t} = D_{DOX}\left(\frac{\partial^2 C_{DOX,i}}{\partial r^2} + \frac{2}{r}\frac{\partial C_{DOX,i}}{\partial r}\right) for\ 2 \le i \le 100 \tag{3.3}$$

This resulted in 99 PDEs describing the change in concentration at each non-boundary node due to diffusion.

Two additional equations were required at the boundary nodes, $C_{DOX,1}$ and $C_{DOX,101}$, to complete the system of differential equations. Mole balances were used to obtain both boundary conditions. At R_1 and at any time *t*, moles of DOX from the aqueous core were lost as DOX diffused into the vesicle bilayer:

$$\frac{\partial\left(C_{DOX,core}V_1\right)}{\partial t} = D_{DOX}\frac{\partial C_{DOX,1}}{\partial r}\bigg|_{R_1} 4\pi {R_1}^2 \tag{3.4}$$

where $C_{DOX,core}$ is the DOX concentration in the Tf-DPEL vesicle aqueous core, and V_1 is the volume of the Tf-DPEL vesicle aqueous core, which was assumed to remain constant. Similarly at R_2 and at any time *t*, moles of DOX in the external buffer were gained as DOX diffused out of the vesicle bilayer:

$$\frac{\partial\left(C_{DOX,ext}\,V_2\right)}{\partial t} = -D_{DOX}\frac{\partial C_{DOX,101}}{\partial r}\bigg|_{R_2} 4\pi {R_2}^2 \tag{3.5}$$

where $C_{DOX,ext}$ is the DOX concentration in the external buffer bath, and V_2 is the constant external buffer volume, which was 1000 mL in our *in vitro* experiments. Both Eqs. (3.4) and

(3.5) are PDEs since multiple independent variables, t and r, are present in the differential equation. However, $C_{DOX,core}$ and $C_{DOX,ext}$ were concentrations in the aqueous solution and not the vesicle bilayer. Since the DOX concentration profile was being solved for within the vesicle bilayer, $C_{DOX,core}$ and $C_{DOX,ext}$ had to be rewritten in terms of membrane concentrations. Assuming that equilibrium was immediately reached at the aqueous-membrane boundary, $C_{DOX,core}$ and $C_{DOX,ext}$ were related to the concentrations in the vesicle membrane by the partition coefficient K. The partition coefficient was defined as the ratio of the DOX concentration in the vesicle membrane to the DOX concentration in an aqueous solution at equilibrium:

$$K \equiv \frac{C_{DOX,mem}}{C_{DOX,aq}} = \frac{C_{DOX,1}}{C_{DOX,core}} = \frac{C_{DOX,101}}{C_{DOX,ext}} \tag{3.6}$$

Equations (3.4) and (3.5) can therefore be simplified to the following:

$$\frac{\partial C_{DOX,1}}{\partial t} = \frac{KD_{DOX}}{V_1} \frac{\partial C_{DOX,1}}{\partial r}\bigg|_{R_1} 4\pi {R_1}^2 \tag{3.7}$$

$$\frac{\partial C_{DOX,101}}{\partial t} = -\frac{KD_{DOX}}{V_2} \frac{\partial C_{DOX,101}}{\partial r}\bigg|_{R_2} 4\pi {R_2}^2 \tag{3.8}$$

Each of the 101 nodes was therefore then described by a PDE with one dependent variable, $C_{DOX,i}$, and two independent variables, t and r.

The method of lines then transformed the system of PDEs into a system of ordinary differential equations (ODEs) by replacing the spatial derivatives, $\frac{\partial C_{DOX,i}}{\partial r}$ and $\frac{\partial^2 C_{DOX,i}}{\partial r^2}$, with finite differences. The first order and second order spatial derivatives of concentration can be rewritten using the centered finite difference approach:

$$\frac{\partial C_{DOX,i}}{\partial r} = \frac{C_{DOX,i+1} - C_{DOX,i-1}}{h} \tag{3.9}$$

$$\frac{\partial^2 C_{DOX,i}}{\partial r^2} = \frac{C_{DOX,i+1} - 2C_{DOX,i} + C_{DOX,i-1}}{h^2} \tag{3.10}$$

The first order spatial derivative can also be rewritten with the forward finite difference:

$$\frac{\partial C_{DOX,i}}{\partial r} = \frac{C_{DOX,,i+1} - C_{DOX,i}}{h} \tag{3.11}$$

or the backward finite difference:

$$\frac{\partial C_{DOX,i}}{\partial r} = \frac{C_{DOX,i} - C_{DOX,i-1}}{h} \tag{3.12}$$

depending on the location of the node being at the initial or final boundary position. These algebraic expressions then replaced the spatial derivatives. When the centered finite differences were applied to the non-boundary nodes described by Eq. (3.3), the PDEs became ODEs since only one independent variable, t, remained as follows:

$$\frac{dC_{DOX,i}}{dt} = D_{DOX}\left(\frac{C_{DOX,i+1}-2C_{DOX,i}+C_{DOX,i-1}}{h^2} + \frac{2}{r}\frac{C_{DOX,i+1}-C_{DOX,i-1}}{h}\right) \quad for\ 2 \le i \le 100 \tag{3.13}$$

The forward finite difference, Eq. (3.11), was applied to Eq. (3.7):

$$\frac{dC_{DOX,1}}{dt} = \frac{KD_{DOX}}{V_1}\left(\frac{C_{DOX,2} - C_{DOX,1}}{h}\right)4\pi {R_1}^2 \tag{3.14}$$

Finally, the backward finite difference, Eq. (3.12), was applied to Eq. (3.8):

$$\frac{dC_{DOX,101}}{dt} = -\frac{D_{DOX}}{V_2}\left(\frac{C_{DOX,101} - C_{DOX,100}}{h}\right)4\pi {R_2}^2 \tag{3.15}$$

Equations (3.13), (3.14), and (3.15) were the 101 ODEs used to numerically solve for the concentration profile.

To accurately capture the *in vitro* release conditions, the system of ODEs was solved twice: once to capture drug release during the 24 hour Tf conjugation period and a second time to predict the release profile during the *in vitro* release experiment. For each release process, the system of ODEs was numerically integrated with respect to time. Therefore, two sets of initial conditions were required to complete the integration.

During the Tf conjugation process, the DPEL vesicles was modeled to have DOX initially loaded homogeneously in V_1 at a concentration C_0. Since we have been assuming that equilibrium is attained between the aqueous phase and the bilayer, the drug immediately partitioned to the first node. The initial condition at node 1 during the conjugation process was given by:

$$C_{DOX,1}\left(t_{conjugation} = 0\right) = KC_0 \tag{3.16}$$

Drug was initially loaded only in the aqueous core, so drug was not initially present at any other node:

$$C_{DOX,i}\left(t_{conjugation} = 0\right) = 0 \; for \; i > 1 \tag{3.17}$$

With these initial conditions, the system of ODEs was numerically integrated using the ode45 solver in MATLAB. This output the DOX concentration at every node as a function of time, and the concentration profile was evaluated at $t = 24$ hours.

The release experiment was similarly modeled. Experimentally, after conjugation, the Tf-DPEL vesicles were placed within the dialysis bag for the release studies. Assuming that the Tf-DPEL vesicles placed in the dialysis bag had an identical DOX concentration profile as the Tf-DPELs after conjugation, the final conditions of the 24 hour conjugation were the initial conditions for modeling the release experiment:

$$C_{DOX,i}\left(t_{conjugation} = 24\right) = C_{DOX,i}(t_{release} = 0)\ for\ all\ i \tag{3.18}$$

where $t_{conjugation}$ represents the time during the 24 hour Tf conjugation process, and $t_{release}$ represents a time in the release study. The system of ODEs was numerically integrated again using the ode45 solver in MATLAB, which output the DOX concentration at every node as a function of time. Drug release was then measured using the assumption that the bilayer-aqueous interface immediately achieved equilibrium. Moles of drug released at any time t were therefore calculated as follows:

$$n_{release}(t_{release}) = C_{DOX,ext}(t_{release})V_2 = \frac{C_{DOX,101}(t_{release})}{K}V_2 \tag{3.19}$$

The initial moles of drug were calculated as:

$$n_{initial} = C_0V_1 + \frac{4}{3}\pi\left[(R_1 + h)^3 - {R_1}^3\right]C_0K \tag{3.20}$$

where C_0V_1 is the initial moles of drug in the aqueous core and $\frac{4}{3}\pi\left[(R_1 + h)^3 - {R_1}^3\right]C_0K$ is the initial moles of drug that immediately partitioned just inside the vesicle bilayer. The percent of drug released after $t_{release}$ hours was calculated as:

$$\%\ drug\ release(t_{release}) = \frac{n_{release}(t_{release})}{n_{initial}} \tag{3.21}$$

3.2.3. *In Vitro* Drug Release Experiment

To prepare for the *in vitro* release experiment, the Tf-DPEL vesicle sample was carefully added to a dialysis bag (MWCO = 10,000 Da). The dialysis bag was then placed in a 1000 mL buffer containing 50 mM HEPES and 20 mM sodium bicarbonate. The release study was performed in a 37°C incubator. At selected time points, 20 µL of the Tf-DPEL vesicle suspension was removed from the dialysis bag, and the DOX concentration was measured as

previously discussed in Chapter 2. Time points were measured every 2 hours for the first 8 hours, and then at 24 hour intervals until 192 hours. Two bath exchanges were performed at 4 hours and 24 hours in order to maintain a low concentration of DOX in the exterior, which in turn, would lead to faster diffusion rates.

3.3. Results and Discussion

3.3.1. Predicted and *In Vitro* Drug Release Profiles for the Tf-DPEL Vesicles

To accurately predict DOX release from the Tf-DPEL vesicles, parameters such as the vesicle core radius R_1, the total radius R_2, the diffusion coefficient of DOX in the vesicle bilayer D_{DOX}, and the initial loading concentration C_0 were determined based on previously measured data or values reported in the literature. First, R_2 was estimated by the DLS measurement presented in Table 2.1. The Tf-DPEL vesicle diameter was approximately 160 nm, so the radius R_2 was set as 80 nm. The inner radius of the vesicle core, R_1, was calculated by subtracting the bilayer thickness from the R_2 value. Kamei and coworkers have previously reported a method for calculating the EL vesicle bilayer thickness [27]. When the $E_{60}L_{20}$ polypeptides self-assemble into vesicles, the polypeptides align such that the hydrophobic membrane has a thickness equal to the length of one hydrophobic L_{20} segment. Since the L_{20} segments form alpha-helices, which typically have 3.6 residues per turn and 5.4 Å per turn, the hydrophobic membrane thickness was calculated as 20 residues multiplied by 5.4 Å per 3.6 residues, equaling 3 nm. The hydrophilic E_{60} segments of adjacent polypeptides face in opposite directions, either inwards or outwards, to create the hydrophilic membranes. The average distance of 3.4 Å per glutamate residue was used to calculate the thickness of the E_{60} segments, which were approximated as random coils. Since two hydrophilic membranes are created by the inward and outward facing E_{60} segments, the collective hydrophilic membrane thickness was 40.8 nm. The entire vesicle membrane was

determined by adding the thickness of the hydrophobic membrane to the hydrophilic membranes, resulting in 43.8 nm. The inner radius of R_1 was then calculated as 36.2 nm.

The DOX diffusion coefficient in the Tf-DPEL vesicle bilayer was selected based on values reported for a similar vesicle system. Eisenberg and coworkers have investigated the release of DOX in polystyrene$_{310}$-*b*-poly(acrylic acid)$_{36}$ (PS$_{310}$-*b*-PAA$_{36}$) vesicles. Since PS$_{310}$-*b*-PAA$_{36}$, which consists of a negatively-charged acrylic acid group and a neutral polystyrene group, self-assemble into vesicles, the EL vesicle bilayer should have similar properties to the PS$_{310}$-*b*-PAA$_{36}$ vesicle bilayer. They reported that the diffusion coefficient for DOX in the PS$_{310}$-*b*-PAA$_{36}$ vesicle polystyrene wall ranged from 8×10^{-17} to 6×10^{-16} cm^2/s [43]. Thus, D_{DOX} values of 1×10^{-17}, 2.5×10^{-17}, 5×10^{-17}, 7.5×10^{-17}, and 1×10^{-16} cm^2/s were investigated for our model.

An initial DOX concentration in the vesicle core, C_0, was selected for each D_{DOX} such that the predicted DOX core concentration after the 24 hour conjugation matched the measured Tf-DPEL DOX concentration, which was 30.4 μg/mL. As shown in Table 3.1, greater C_0 values were required as D_{DOX} increased. This makes sense since a larger D_{DOX} translates to a faster DOX mobility in the vesicle bilayer, and therefore faster DOX release. Therefore, larger C_0 values were required with larger D_{DOX} values such that the core concentration dropped to approximately 30.4 μg/mL.

Table 3.1: A table of the parameter values used for D_{DOX} and C_0, and the resulting aqueous core DOX concentration values after conjugation.

Table 3.1		
Diffusion Coefficient D_{DOX} (cm^2/s)	**Initial DOX Concentration C_0 (μg/mL)**	**Predicted Aqueous Core DOX Concentration After Conjugation (μg/mL)**
$1 * 10^{-17}$	60	30.1
$2.5 * 10^{-17}$	120	30.3
$5 * 10^{-17}$	225	30.7
$7.5 * 10^{-17}$	365	30.3
$1 * 10^{-16}$	590	30.2

After compiling the parameter values, the DOX concentration profile was numerically solved to model the release study, and the percent drug released was calculated at the time points that corresponded to the *in vitro* experiment. Both the predicted release profiles and the *in vitro* release profile were plotted in Figure 3.2 for comparison. The *in vitro* release data is plotted in black while the predicted release data are plotted in blue, red, green, yellow, and orange for D_{DOX} values of 1×10^{-17}, 2.5×10^{-17}, 5×10^{-17}, 7.5×10^{-17}, and 1×10^{-16} cm^2/s, respectively.

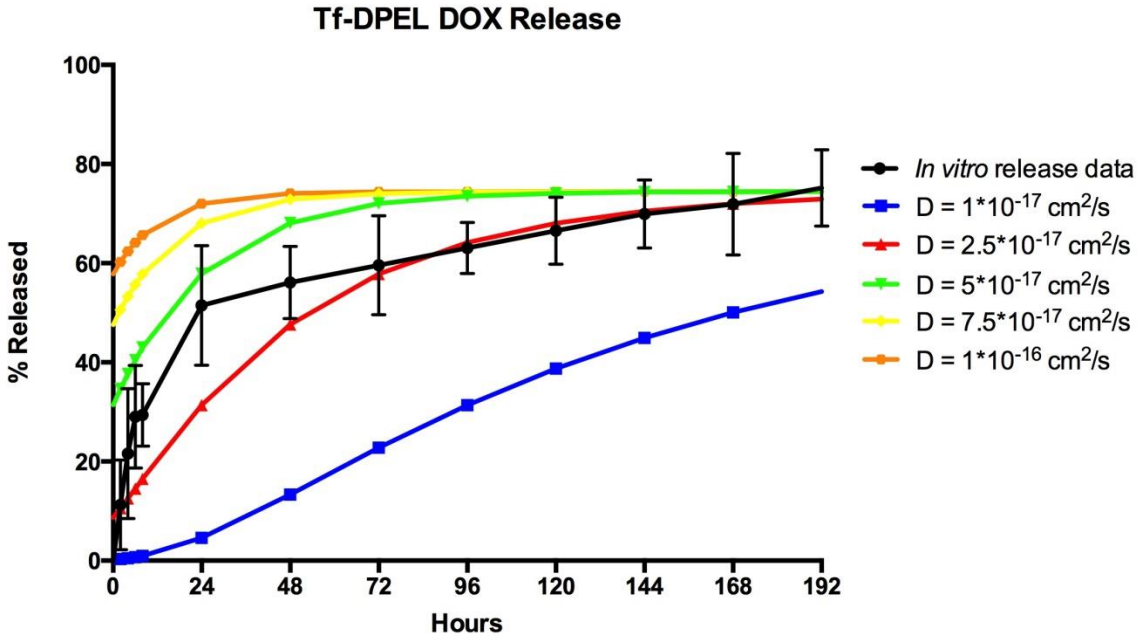

Figure 3.2: The *in vitro* release profile and the predicted release profile were plotted for 192 hours. The *in vitro* release data are shown with the black data points, while the predicted release data are plotted in blue, red, green, yellow, and orange for D_{DOX} values of 1×10^{-17}, 2.5×10^{-17}, 5×10^{-17}, 7.5×10^{-17}, and 1×10^{-16} cm^2/s, respectively.

For the *in vitro* release profile, 63% of the DOX was released after 96 hours. A fast initial release was observed with 51.5% of the DOX being released after the first 24 hours. This burst release was most likely due to some of the drug being adsorbed at the outer surface of the vesicle bilayer. At the start of the release study, the bilayer drug was quickly released compared to the

drug in the aqueous core. After the burst release, DOX steadily released from t=24 hours until t=192 hours where 75.2% of the drug was released. This steady release may be due to the DOX-sulfate gel-like complexes in the aqueous core. DOX must also first dissociate from the sulfate anion in order to travel across the vesicle bilayer.

Our mathematical model accurately predicted the *in vitro* release profile. Note that $D_{DOX} = 1 \times 10^{-17}$ cm^2/s was the smallest diffusion coefficient value tested. A smaller diffusion coefficient translates to a slower mobility of DOX molecules in the vesicle bilayer. Therefore, it made sense that this resulted in a steady release profile with only 54.3% released after 192 hours. As D_{DOX} was increased, the release profile exhibited a quick burst release since a larger diffusion coefficient translates to a faster release. Additionally, the release profiles with larger D_{DOX} values closely converged to the percent released at 192 hours for the *in vitro* release profile. When $D_{DOX} = 1 \times 10^{-16}$ cm^2/s, 74.4% of the drug was released after 192 hours compared to 75.2% in the *in vitro* release. The *in vitro* release profile sits between the predicted release profiles for $D_{DOX} = 2.5 \times 10^{-17}$ cm^2/s and $D_{DOX} = 5 \times 10^{-17}$ cm^2/s, which are reasonable estimates for the diffusion coefficient.

It should be noted that all of the predicted release profiles have released some DOX at $t_{release} = 0$, which is not possible *in vitro,* and this was due to our drug release calculation. The mathematical model predicted that $C_{DOX,101}(t_{conjugation} = 24)$ will have a big effect since DOX had diffused to the 101st node after the 24 hour Tf conjugation process. Subsequently, the DOX concentration profile at $t_{conjugation} = 24$ was used as the initial condition for $t_{release} = 0$, *i.e.*, $C_{DOX,101}(t_{conjugation} = 24) = C_{DOX,101}(t_{release} = 0)$. We calculated drug release by assuming the immediate partitioning of the drug to the external buffer, so $n_{release}(t_{release} = 0)$ also had some value. Therefore, our model predicted that drug was already released at $t_{release} =$

0. For $D_{DOX} = 1 \times 10^{-17}$ cm^2/s, the percent released at $t_{release} = 0$ was 0.208%. DOX diffused outwards slowly. Since the diffusion coefficient was small, not much of the drug reached the 101st node after the 24 hour conjugation. Thus, little drug partitioned to the external buffer at the start of the release model. When D_{DOX} increased to 1×10^{-16} cm^2/s, greater amounts of DOX diffused to the 101st node after the 24 hour conjugation, so 57.8% of drug was released at $t_{release} = 0$ due to the partitioning. Although this is not feasible *in vitro*, this unexpectedly captured the burst release characteristic exhibited by the *in vitro* release profile.

4. Drug Delivery Efficacy of the Tf-DPEL Vesicles

4.1. Motivation and Background

In vivo studies have been widely used to determine the effects of therapeutic agents on animals as these assays allow for further analysis of the drug's actions on organs and tissue. The animal's recovery can also be monitored for extended periods of time [44]. However, *in vivo* testing is strictly regulated, requires extensive training, and is costly to perform [44]. Therefore, there has been a shift in interest towards *in vitro* cytotoxicity assays to determine the cytotoxic effects of therapeutic agents. These assays are beneficial as cell culture is time and cost-effective compared to *in vivo* tests, *in vitro* methods do not require personnel experienced in animal handling, and they can rapidly screen the toxic effects of multiple molecules to reduce unnecessary *in vivo* testing [45].

In vitro cytotoxicity assays are typically performed by incubating the therapeutic agents with the cells for a desired duration, often 72 to 96 hours. Afterwards, cell viability is measured, and one common assay in the cancer therapy field is the 3-(4,5-dimethylthiazol-2-yl)-5-(3-carboxymethoxyphenyl)-2(4-sulfonyl)-2H-tetrazolium (MTS) assay. MTS is a substrate that is converted to a colored formazan product by live cells since the reduction reaction occurs using succinate dehydrogenase only in functional mitochondria [46]. The water-soluble formazan is then released to the medium where it can be measured by absorbance to determine cell viability. A greater measured absorbance value corresponds to a greater number of cells that have survived during the *in vitro* cytotoxicity assay.

In this chapter, we will be discussing the *in vitro* cytotoxicity of the Tf-DPEL vesicles in PC3 human prostate cancer cells. We expected an improved drug delivery efficacy with the Tf-DPEL vesicles compared to the non-targeted DPEL vesicles since the non-targeted DPEL

vesicles do not have a mechanism to enter the cell. Accordingly, the DPEL vesicles were expected to exhibit cell death only by releasing DOX in the extracellular environment. On the other hand, the Tf-DPEL vesicles are conjugated to the Tf targeting ligand, allowing the Tf-DPEL vesicles to be internalized by the cancer cells via receptor-mediated endocytosis. Upon entering the cell, the Tf-DPEL vesicle can release its drug intracellularly, resulting in greater cell death.

4.2. Materials and Methods

4.2.1. Materials

The PC3 cell line was obtained from the American Type Culture Collection (Manassas, Virginia). Roswell Park Memorial Institute (RPMI) 1640 medium, penicillin-streptomycin (P/S), sodium pyruvate (NaPyr), phosphate-buffered saline (PBS), and 0.25% trypsin with ethylenediaminetetraacetic acid **(**EDTA) were purchased from Invitrogen (Carlsbad, California). Fetal bovine serum (FBS) was obtained from Hyclone (Waltham, Massachusetts). Dialysis bags (MWCO = 1,000 Da) were purchased from Spectrum Laboratories (Rancho Dominguez, California). The CellTiter 96® AQueous Non-radioactive Cell Proliferation Assay (MTS assay) was purchased from Promega (Madison, Wisconsin).

4.2.2. Cell Culture

The PC3 prostate cancer cell line was grown in RPMI 1640 media supplemented with 10% FBS and 1% P/S. These cells were maintained in a 37˚C humidified atmosphere with 5% CO_2 and passaged with standard cell culture protocols.

4.2.3. *In Vitro* Cytotoxicity Assay

One day prior to the cytotoxicity experiment, PC3 cells were seeded on a 96-well plate at a density of 7,500 cells/cm^2. After allowing the cells to grow overnight, the growth medium was aspirated. Tf-DPEL vesicles were added to RPMI 1640 medium with DOX concentrations varying from 0.01 to 3.16 μM. 100 μL of a suspension containing vesicles in the growth medium were then added to each well. After a 96-hour incubation period, the cell viability was determined with an MTS assay. Cell viability relative to the control (PC3 cells incubated in media without vesicles) was quantified by measuring the absorbance values at 490 and 700 nm. Cell growth inhibition was then compared against that of the non-targeted DPEL vesicles to evaluate the killing efficiency of the targeted vesicles.

4.2. Results and Discussion

4.2.1. Drug Delivery Efficacy of the Tf-DPEL Vesicle

To mimic the *in vivo* conditions of TfR overexpression on cancer cells, the PC3 human prostate cancer cell line was used for the cytotoxicity studies. PC3 cells exhibit TfR levels comparable to their *in vivo* expression, which are 10-fold greater than that of human benign prostatic hyperplasia specimens [47]. The Tf-DPEL vesicles and their non-targeted counterpart, the DPEL vesicles, were administered to the PC3 prostate cancer cells over a range of concentrations for 96 hours. Cell viability was determined using the MTS assay.

The Tf-DPEL vesicles exhibited an improved drug delivery efficacy, since for every percent of cellular growth inhibition, a lower drug concentration was required for the Tf-DPEL vesicles than the DPEL vesicles to achieve the same percent inhibition (Figure 4.1). The IC_{50} value, which is the concentration of drug required to achieve 50% cell inhibition, of the Tf-DPEL and DPEL vesicles were 0.087 and 0.133 μM, respectively, corresponding to a 1.53-fold

difference. Accordingly, fewer Tf-DPEL vesicles were required to achieve a 50% growth inhibition.

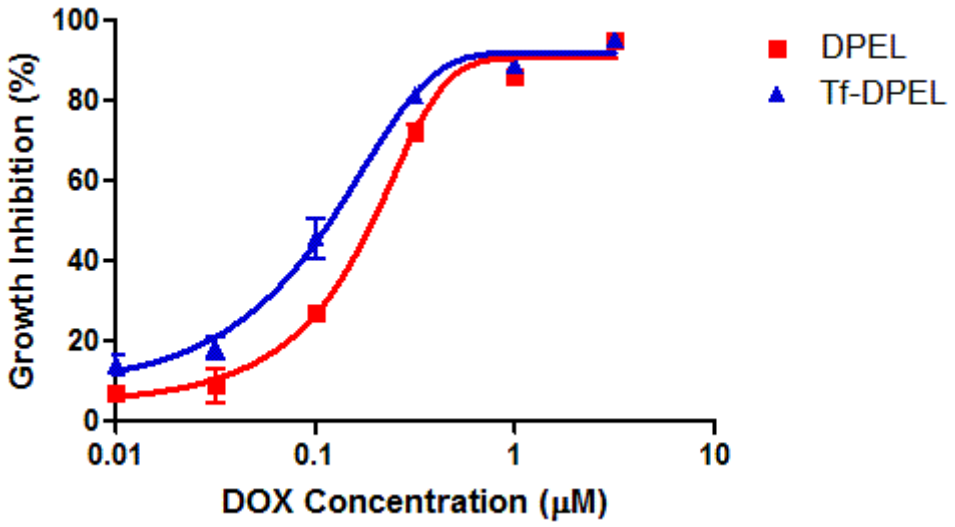

Figure 4.1: *In vitro* cytotoxicity results for the DPEL and Tf-DPEL vesicles in PC3 cells. The IC_{50} value of the DPEL was 0.133 µM, and the IC_{50} value of the Tf-DPEL was 0.087 µM.

Although the DPEL vesicles had no method of entering the cancer cells, the DPEL vesicles still could exert cell growth inhibition as the encapsulated DOX could be released in the extracellular environment, diffuse across the cell phospholipid bilayer, and reach its intracellular target. However, this killing contribution was also present in the Tf-DPEL vesicles since they also released DOX in the extracellular environment when they were not internalized in the cell. Since the presence of Tf was the only variation between the Tf-DPEL and the DPEL vesicles, the increased percent growth inhibition was most likely due to the targeting characteristics of Tf. Upon entering the cell via receptor-mediated endocytosis, the Tf-DPEL vesicles were able to release the encapsulated DOX directly within the cell, and this released DOX could subsequently enter the nucleus and exert its cytotoxic effects.

5. Appendix

5.1. Analytical Solution to Fick's Second Law

We obtained an analytical solution to Fick's Second Law, *i.e.*, a simplified form of the Conservation of Species equation for mass transfer, to describe DOX diffusion in the Tf-DPEL vesicle bilayer. This method provided an analytical solution rather than a numerical one. Recall that Fick's Second Law can be written in spherical coordinates as follows:

$$\frac{\partial C_{DOX,mem}(r,t)}{\partial t} = D_{DOX}\frac{1}{r^2}\frac{\partial}{\partial r}\left(r^2\frac{\partial C_{DOX,mem}(r,t)}{\partial r}\right) \tag{5.1.1}$$

where $C_{DOX,mem}$ is the concentration of DOX in the membrane, t is time, and r is the radial distance from the center of the vesicle. D_{DOX} is the diffusion coefficient of DOX in the membrane, which is a physical parameter that describes the mobility of DOX in the Tf-DPEL vesicle membrane. For our model, D_{DOX} was assumed to remain constant throughout the entire Tf-DPEL vesicle bilayer. Additionally, it was assumed that DOX was dilute in the bilayer such that DOX only interacts with the membrane and not with other DOX molecules. Since $C_{DOX,mem}$ depends on two independent variables, t and r, the differential equation is a partial differential equation (PDE).

In order to solve the PDE, two boundary conditions and an initial condition are required. We modeled the TF-DPEL vesicle as one with an inner aqueous core radius of R_1 and an overall radius of R_2 at the outermost boundary of the vesicle. Our analysis assumed that drug was initially loaded homogeneously within the aqueous core and was not initially present anywhere else. One boundary condition that we used stated that the concentration in the aqueous core for all times is C_0. Since the DOX diffusion problem was solved for in the vesicle membrane, we

used the partition coefficient to relate the aqueous core concentration to the concentration just inside the vesicle bilayer:

$$K \equiv \frac{C_{DOX,mem}}{C_{DOX,aq}} \tag{5.1.2}$$

Thus, the boundary condition at R_1 is given by:

$$C_{DOX,mem}(R_1, t) = KC_0 \tag{5.1.3}$$

DOX was not present in the external buffer, so the DOX concentration in the external buffer was 0. Relating the external DOX concentration to the DOX concentration at R_2 through the partition coefficient gives us our second boundary condition:

$$C_{DOX,mem}(R_2, t) = 0 \tag{5.1.4}$$

Finally, our initial condition stated that, for all positions, the concentration at the initial time is 0:

$$C_{DOX,mem}(r, 0) = 0 \tag{5.1.5}$$

Unfortunately, these boundary conditions and initial condition are not representative of the *in vitro* system since the boundary conditions corresponded to constant concentrations in the aqueous core and the external buffer. In reality, the DOX concentration in the core decreased as DOX was released over time, and the DOX concentration in the external buffer increased. Despite this deviation from the experiment, we continued with the derivation to determine if the analytical solution would still yield reasonable results.

Prior to analytically solving this PDE, we introduced a new variable $v(r, t)$, which was defined as r multiplied by $C_{DOX,mem}(r, t)$:

$$v(r, t) \equiv rC_{DOX,mem}(r, t) \tag{5.1.6}$$

and $v(r,t)$ was therefore also a dependent variable that was a function of t and r. Using Eq. (5.1.6), Eq. (5.1.1) becomes:

$$\frac{\partial}{\partial t}\left(\frac{v(r,t)}{r}\right) = D_{DOX}\frac{1}{r^2}\frac{\partial}{\partial r}\left[r^2\frac{\partial}{\partial r}\left(\frac{v(r,t)}{r}\right)\right] \tag{5.1.7}$$

The product rule is then performed on Eq. (5.1.7), and further simplified to yield:

$$\frac{\partial v(r,t)}{\partial t} = D_{DOX}\frac{\partial^2 v(r,t)}{\partial r^2} \tag{5.1.8}$$

Equation (5.1.8) is now a PDE with the dependent variable $v(r,t)$ and the same independent variables t and r. The substitution for $C_{DOX,mem}(r,t)$ allowed us to remove the additional terms that arose from spherical coordinates, and the new PDE resembled Fick's Second Law in Cartesian coordinates, which is easier to solve. We then converted the boundary conditions and initial condition for the new dependent variable. Using the definition for $v(r,t)$, the boundary condition at R_1 can be rewritten as:

$$v(R_1,t) = R_1 K C_0 \equiv v_0 \tag{5.1.9}$$

Similarly for the boundary condition at R_2, Eq. (5.1.4) can be rewritten as follows:

$$v(R_2,t) = 0 \tag{5.1.10}$$

Finally, the initial condition can be rewritten as follows:

$$v(r,0) = 0 \tag{5.1.11}$$

It should be noted that the following derivation was not available in the literature, and only the final concentration profile and the drug release equation were provided in another review paper for confirmation. The finite fourier transform (FFT) was used to analytically solve for the PDE in Eq. (5.1.8). We first solved for $v(r,t)$ and then converted it back to

$C_{DOX,mem}(r,t)$ using its definition. According to the FFT method, the final solution is assumed to be a product of two functions where each function is dependent on a single variable:

$$v(r,t) = \sum_{n=1}^{\infty} \theta_n(t)\emptyset_n(r) \tag{5.1.12}$$

where $\emptyset_n(r)$ is known as the basis function and is dependent on the position variable:

$$\emptyset_n(r) = \sqrt{\frac{2}{R_2 - R_1}} \sin\left(n\pi \frac{r - R_1}{R_2 - R_1}\right) \tag{5.1.13}$$

There are multiple basis functions that one can select based on the problem's boundary conditions. This particular basis function was selected as it satisfies our boundary conditions, which corresponded to the concentration values at the two boundaries. For example, if our boundary condition consisted of a diffusional flux instead of a concentration value, then a different basis function would be required. The second function, $\theta_n(t)$, is a function dependent on the variable time and is equal to:

$$\theta_n(t) = \int_{R_1}^{R_2} v(r,t)\,\emptyset_n(r)dr \tag{5.1.14}$$

To determine $v(r,t)$, we multiply $\theta_n(t)$ with $\emptyset_n(r)$, and take the summation from $n = 1$ to ∞. We already have an expression for the basis function $\emptyset_n(r)$, which was selected based on our boundary conditions. Therefore, we needed to determine an expression for $\theta_n(t)$ to complete our solution. To find $\theta_n(t)$, we began by transforming Eq. (5.1.8) by multiplying both sides by the basis function and then integrating with respect to r from R_1 to R_2, which are the positional boundaries of our diffusion problem:

$$\int_{R_1}^{R_2} \frac{\partial v(r,t)}{\partial t} \emptyset_n(r) dr = \int_{R_1}^{R_2} D_{DOX} \frac{\partial^2 v(r,t)}{\partial r^2} \emptyset_n(r) dr \tag{5.1.15}$$

We can define the left side of Eq. (5.1.15) as P_1, which is also equal to the derivative of $\theta_n(t)$ with respect to time:

$$P_1 \equiv \int_{R_1}^{R_2} \frac{\partial v(r,t)}{\partial t} \emptyset_n(r) dr = \frac{d\theta_n(t)}{dt} \tag{5.1.16}$$

We can define the right side of Eq. (5.1.15) as P_2:

$$P_2 \equiv \int_{R_1}^{R_2} D_{DOX} \frac{\partial^2 v(r,t)}{\partial r^2} \emptyset_n(r) dr \tag{5.1.17}$$

Therefore, Eq. (5.1.15) can be rewritten as:

$$P_1 = P_2 \tag{5.1.18}$$

Let us first focus on P_2 and determine this expression. The integral with respect to r consists of the product of two functions dependent on the variable r. Therefore, to solve this integral, we must integrate by parts. Integration by parts allows us to relate the integral of a product of functions to the functions' derivative and antiderivative:

$$\int_{R_1}^{R_2} u(r)\, dV(r) dr = u(r)V(r)\Big|_{R_1}^{R_2} - \int_{R_1}^{R_2} V(r)\, du(r) dr \tag{5.1.19}$$

$u(r)$ and $V(r)$ are both functions dependent on r. For Eq. (5.1.17), $u(r)$ and $dV(r)$ are selected as follows:

$$u = \emptyset_n(r) \qquad du = \frac{d\emptyset_n(r)}{dr} dr \tag{5.1.20}$$

$$dV = \frac{\partial^2 v(r,t)}{\partial r^2} dr \qquad V = \frac{\partial v(r,t)}{\partial r} \tag{5.1.21}$$

Performing the integration by parts on Eq. (5.1.17) leads to:

$$P_2 = D_{DOX}\left[\left(\emptyset_n(r)\frac{\partial v(r,t)}{\partial r}\Big|_{R_1}^{R_2}\right) - \int_{R_1}^{R_2}\frac{\partial v(r,t)}{\partial r}\frac{d\emptyset_n(r)}{dr}dr\right] \tag{5.1.22}$$

The integration term in Eq. (5.1.22) again consists of an integral of the product of two functions. Therefore, integration by parts is performed again. The $u(r)$ and $dV(r)$ terms are selected as follows:

$$u = \frac{d\emptyset_n(r)}{dr} \qquad du = \frac{d^2\emptyset_n(r)}{dr^2}dr \tag{5.1.23}$$

$$dV = \frac{\partial v(r,t)}{\partial r}dr \qquad V = v(r,t) \tag{5.1.24}$$

The second integration by parts results in:

$$P_2 = D_{DOX}\left[\left(\emptyset_n(r)\frac{\partial v(r,t)}{\partial r}\Big|_{R_1}^{R_2}\right) - \left(\frac{d\emptyset_n(r)}{dr}v(r,t)\Big|_{R_1}^{R_2}\right) + \int_{R_1}^{R_2} v(r,t)\frac{d^2\emptyset_n(r)}{dr^2}dr\right] \tag{5.1.25}$$

The bounds of integration are then evaluated, resulting in:

$$P_2 = D_{DOX}\left(\emptyset_n(R_2)\frac{\partial v(r,t)}{\partial r}\Big|_{r=R_2} - \emptyset_n(R_1)\frac{\partial v(r,t)}{\partial r}\Big|_{r=R_1} - v(r=R_2,t)\frac{d\emptyset_n(r)}{dr}\Big|_{r=R_2} + v(r=R_1,t)\frac{d\emptyset_n(r)}{dr}\Big|_{r=R_1} + \int_{R_1}^{R_2} v(r,t)\frac{d^2\emptyset_n(r)}{dr^2}dr\right) \tag{5.1.26}$$

To evaluate Eq. (5.1.26), we must first obtain the first order and second order derivatives of $\emptyset_n(r)$ with respect to r. The first order derivative of $\emptyset_n(r)$ with respect to r is:

$$\frac{d\emptyset_n(r)}{dr} = \frac{\sqrt{2}n\pi}{(R_2 - R_1)^{3/2}} \cos\left(n\pi \frac{r - R_1}{R_2 - R_1}\right) \tag{5.1.27}$$

The second order derivative of $\emptyset_n(r)$ with respect to r is:

$$\frac{d^2\emptyset_n(r)}{dr^2} = -\frac{\sqrt{2}n^2\pi^2}{(R_2 - R_1)^{5/2}} \sin\left(n\pi \frac{r - R_1}{R_2 - R_1}\right) = -\frac{n^2\pi^2}{{R_2 - R_1}^2} \emptyset_n(r) \tag{5.1.28}$$

We can recognize that many terms in Eq. (5.1.26) are equal to 0. Specifically, $\emptyset_n(R_2) = 0$ and $\emptyset_n(R_1) = 0$ according to the basis function and $v(r = R_2, t) = 0$ according to one of the boundary conditions. Thus, evaluating the bounds of integrations for Eq. (5.1.26) and simplifying yields:

$$P_2 = D_{DOX}\left[\frac{\sqrt{2}n\pi v_0}{(R_2 - R_1)^{3/2}} - \frac{n^2\pi^2}{(R_2 - R_1)^2}\theta_n(t)\right] \tag{5.1.29}$$

Since $P_1 = P_2$ according to Eq. (5.1.18), replacing P_1 with Eq. (5.1.16) and P_2 with Eq. (5.1.29) and rearranging terms yields:

$$\frac{d\theta_n(t)}{dt} + \frac{D_{DOX}n^2\pi^2}{(R_2 - R_1)^2}\theta_n(t) = \frac{\sqrt{2}D_{DOX}n\pi v_0}{(R_2 - R_1)^{3/2}} \tag{5.1.30}$$

Equation (5.1.30) has now been transformed to an ordinary differential equation with the dependent variable $\theta_n(t)$ and one independent variable t. To complete the integration of the ODE for $\theta_n(t)$, we require an initial condition for $\theta_n(t)$. The definition for $\theta_n(t = 0)$,which was defined in Eq. (5.1.14), becomes:

$$\theta_n(t = 0) = \int_{R_1}^{R_2} v(r, 0)\, \emptyset_n(r) dr = 0 \tag{5.1.31}$$

since $v(r,0) = 0$ according to our initial condition for $v(r,t)$. The ODE can then be solved using an integrating factor, which is a function that makes the differential equation integrable. The integrating factor is equal to:

$$IF = exp\left(\int \frac{D_{DOX}n^2\pi^2}{(R_2 - R_1)^2}dt\right) = exp\left(\frac{D_{DOX}n^2\pi^2}{(R_2 - R_1)^2}t\right) \tag{5.1.32}$$

Using the integrating factor,

$$\frac{d}{dt}[\theta_n(t) \cdot IF] = \frac{\sqrt{2}D_{DOX}n\pi v_0}{(R_2 - R_1)^{\frac{3}{2}}} \cdot IF \tag{5.1.33}$$

Integrating both sides of Eq. (5.1.33) with respect to time results in:

$$\theta_n(t)exp\left(\frac{D_{DOX}n^2\pi^2}{(R_2 - R_1)^2}t\right) = \frac{\sqrt{2}(R_2 - R_1)^{\frac{1}{2}}v_0}{n\pi}exp\left(\frac{D_{DOX}n^2\pi^2}{(R_2 - R_1)^2}t\right) + B \tag{5.1.34}$$

where B is the constant of integration. The initial condition stated in Eq. (5.1.31) is used to solve for B. After solving for the constant of integration and dividing both sides by the integrating factor, the solution for $\theta_n(t)$ becomes:

$$\theta_n(t) = \frac{\sqrt{2}(R_2 - R_1)^{\frac{1}{2}}v_0}{n\pi}\left[1 - exp\left(-\frac{D_{DOX}n^2\pi^2}{(R_2 - R_1)^2}t\right)\right] \tag{5.1.35}$$

Recall that the overall solution for $v(r,t)$ was the summation of the product of the two functions, $\theta_n(t)$ and $\emptyset_n(r)$, from $n = 1$ to ∞. We previously determined $\emptyset_n(r)$ by selecting the correct basis function based on our boundary conditions. We just determined an expression for $\theta_n(t)$ in Eq. (5.1.35). Therefore, we can determine the solution for $v(r,t)$:

$$v(r,t) = \sum_{n=1}^{\infty}\frac{2v_0}{n\pi}\sin\left(n\pi\frac{r-R_1}{R_2-R_1}\right) - \frac{2v_0}{n\pi}exp\left(-\frac{D_{DOX}n^2\pi^2}{(R_2-R_1)^2}t\right)\sin\left(n\pi\frac{r-R_1}{R_2-R_1}\right) \tag{5.1.36}$$

Equation (5.1.36) can be further simplified by the Fourier sine series:

$$1 - X = 2\sum_{n=1}^{\infty} \frac{\sin(n\pi X)}{n\pi} \tag{5.1.37}$$

When X is replaced with $\frac{r-R_1}{R_2-R_1}$ to match the variable within our sine term, the Fourier sine series can be written as follows:

$$1 - \frac{r - R_1}{R_2 - R_1} = 2\sum_{n=1}^{\infty} \frac{\sin\left(n\pi \frac{r - R_1}{R_2 - R_1}\right)}{n\pi} \tag{5.1.38}$$

Thus, after replacing the Fourier sine series and simplifying, Eq. (5.1.36) becomes:

$$v(r,t) = \frac{v_0(R_2 - r)}{(R_2 - R_1)} - \frac{2}{\pi}\sum_{n=1}^{\infty} \frac{v_0}{n} exp\left(-\frac{D_{DOX}n^2\pi^2}{(R_2 - R_1)^2}t\right)\sin\left(n\pi \frac{r - R_1}{R_2 - R_1}\right) \tag{5.1.39}$$

Equation (5.1.39) is the analytical solution for the PDE in Eq. (5.1.8). However, we ultimately want $C_{DOX,mem}(r,t)$. Earlier, we defined $v(r,t) \equiv rC_{DOX,mem}(r,t)$ in Eq. (5.1.6). Therefore, we complete our analytical solution for $C_{DOX,mem}(r,t)$ by dividing Eq. (5.1.39) by r:

$$C_{DOX,mem}(r,t) = \frac{R_1KC_0(R_2-r)}{(R_2-R_1)r} - \frac{2}{\pi}\sum_{n=1}^{\infty} \frac{R_1KC_0}{nr} exp\left(-\frac{D_{DOX}n^2\pi^2}{(R_2-R_1)^2}t\right)\sin\left(n\pi \frac{r-R_1}{R_2-R_1}\right) \tag{5.1.40}$$

Wang and coworkers have reported the same analytical solution for the unsteady state diffusion problem with Fick's Second Law in spherical coordinates as we have derived in Eq. (5.1.40) [41].

Now that we have a concentration profile for DOX in the vesicle bilayer, we can evaluate the flux of drug per time across any surface area of the vesicle bilayer. The units of the flux are moles per surface area per time. Therefore, multiplying the flux by the surface area gives us the moles of drug released per time across this surface area: The flux is evaluated as follows:

$$J|_r 4\pi r^2 = -D_{DOX} \left. \frac{\partial C_{DOX,mem}(r,t)}{\partial r} \right|_r \tag{5.1.41}$$

After taking the derivative of the concentration profile, Eq. (5.1.41) becomes:

$$J|_r 4\pi r^2 =$$

$$\frac{4\pi D_{DOX} R_1 R_2 K C_0}{(R_2 - R_1)} - 8\sum_{n=1}^{\infty} \frac{D_{DOX_1} R_1 K C_0}{n} exp\left(-\frac{D_{DOX} n^2 \pi^2}{(R_2-R_1)^2} t\right) \left[\frac{rn\pi}{(R_2-R_1)} \cos\left(n\pi \frac{r-R_1}{R_2-R_1}\right) - \right. \tag{5.1.42}$$

$$\left. \sin\left(n\pi \frac{r-R_1}{R_2-R_1}\right)\right]$$

Finally, we can determine the moles of drug released across the surface area $4\pi r^2$ after some time t by taking the integral of Eq. (5.1.42) with respect to time:

$$\int_0^t J|_r 4\pi r^2 \, dt =$$

$$\frac{4\pi D_{DOX} R_1 R_2 K C_0}{(R_2 - R_1)} t - 8\sum_{n=1}^{\infty} \frac{D_{DOX_1} R_1 K C_0}{n} exp\left(-\frac{D_{DOX} n^2 \pi^2}{(R_2-R_1)^2} t\right) \left[\frac{rn\pi}{(R_2-R_1)} \cos\left(n\pi \frac{r-R_1}{R_2-R_1}\right) - \right. \tag{5.1.43}$$

$$\left. \sin\left(n\pi \frac{r-R_1}{R_2-R_1}\right)\right]$$

In the *in vitro* release experiment, we are measuring drug that has left the vesicle bilayer at R_2. Therefore, we wish to measure the drug release across the surface area at R_2. Replacing r with R_2 in Eq. (5.1.43) gives us the amount of drug that has been released from the entire vesicle after some time t:

$$n_{released}(t) = \int_0^t J|_{r=R_2} 4\pi {R_2}^2 = 4\pi D_{DOX} R_1 R_2 K C_0 \left[\frac{D_{DOX_1}}{(R_2-R_1)^2} t + \frac{2}{\pi^2}\sum_{n=1}^{\infty} \frac{(-1)^n}{n^2} - \right. \tag{5.1.44}$$

$$\left. \frac{2}{\pi^2}\sum_{n=1}^{\infty} \frac{(-1)^n}{n^2} exp\left(-\frac{D_{DOX} n^2 \pi^2}{(R_2-R_1)^2} t\right)\right]$$

Finally, we determined that the infinite series $\sum_{n=1}^{\infty} \frac{(-1)^n}{n^2}$ converges to a finite value, specifically, we confirmed with MATLAB that:

$$\sum_{n=1}^{\infty} \frac{(-1)^n}{n^2} = -\frac{\pi^2}{12} \tag{5.1.45}$$

Thus, Eq. (5.1.44) is simplified to:

$$n_{released}(t) = 4\pi D_{DOX} R_1 R_2 K C_0 \left[\frac{D_{DOX_1}}{(R_2 - R_1)^2} t - \frac{1}{6} - \frac{2}{\pi^2} \sum_{n=1}^{\infty} \frac{(-1)^n}{n^2} exp\left(-\frac{D_{DOX} n^2 \pi^2}{(R_2 - R_1)^2} t \right) \right] \tag{5.1.46}$$

To confirm that our drug release equation is mathematically correct, we have derived the same solution as the cumulative drug release equation for spherical systems also reported by Wang and coworkers [41]. The predictions from this model varied from our experimentally measured values, which wasn't surprising due to the assumptions of constant concentrations in the two aqueous solutions.

5.2. Pseudo-Steady Analysis to Fick's Second Law

We also predicted drug release by solving Fick's Second Law (i.e., a simplified form of the Conservation of Species equation describing mass transfer) using the pseudo-steady analysis. Recall that Fick's Second Law can be written in spherical coordinates as follows:

$$\frac{\partial C_{DOX,mem}}{\partial t} = D_{DOX} \frac{1}{r^2} \frac{\partial}{\partial r} \left(r^2 \frac{\partial C_{DOX,mem}}{\partial r} \right) \tag{5.2.1}$$

where $C_{DOX,mem}$ is the concentration of DOX in the membrane, t is time, and r is the radius measured from the center of the vesicle. D_{DOX} is the diffusion coefficient of DOX in the membrane, which is a physical parameter that describes the mobility of DOX in a Tf-DPEL vesicle membrane. For our model, D_{DOX} was assumed to remain constant throughout the entire Tf-DPEL vesicle bilayer. Additionally, it was assumed that DOX was dilute in the bilayer such

that DOX only interacts with the membrane and not with other DOX molecules. In the differential equation, $C_{DOX,mem}$ depends on two independent variables, t and r.

DOX is modeled to be initially present only in the aqueous core. As DOX is released from the aqueous core, it diffuses across the vesicle bilayer and eventually exits to the external buffer. Thus, the DOX concentration in the external buffer will increase as the DOX concentration in the core decreases. According to the pseudo-steady analysis, we assume that the DOX concentration in the two compartments, the aqueous core and the external buffer, change very slowly with time. Additionally, we assume that DOX diffusion is very fast such that DOX diffusion in the bilayer is treated as steady-state problem. This can be described by the following situation. At $t = 0$, the concentration in the core is $C_{core}(t = 0)$ and the concentration in the external buffer is $C_{ext}(t = 0) = 0$. Since the concentrations change very slowly, these concentrations can be seen as constant in the diffusion problem. DOX diffuses outwards due to the concentration gradient, but DOX diffusion in the bilayer is treated as being extremely fast relative to the rate at which the concentrations in the aqueous solutions change. Steady-state diffusion is therefore assumed, and the concentration profile is predicted for $C_{core}(t = 0)$ and $C_{ext}(t = 0) = 0$. After some time t_1, DOX has diffused out such that C_{core} has decreased incrementally, and C_{ext} has increased incrementally. Now at t_1, the concentration in the core is $C_{core}(t_1)$, and the concentration in the external buffer is $C_{ext}(t_1)$. Again, the concentrations change very slowly and DOX diffusion is very fast, so the diffusion problem at t_1 is treated as being at steady-state. After the steady-state concentration profile is obtained, C_{core} decreases incrementally and C_{ext} increases incrementally, and this process is repeated until equal concentrations exist inside the core and in the external buffer.

This scenario allows us to assume a steady-state diffusion problem to simplify Eq. (5.2.1) to the following equation:

$$0 = D_{DOX}\frac{1}{r^2}\frac{\partial}{\partial r}\left(r^2\frac{\partial C_{DOX,mem}}{\partial r}\right) \tag{5.2.2}$$

Although Eq. (5.2.2) only consists of a differential equation with respect to one independent variable r, the partial derivative notation remains as the time dependence will be introduced in the boundary conditions. Two boundary conditions are required to complete the integration of Eq. (5.2.2). The two boundary conditions in the vesicle bilayer are related to the core concentration and the external concentration by the partition coefficient as defined in Chapter 3:

$$K \equiv \frac{C_{DOX,mem}}{C_{DOX,aq}} = \frac{C_{DOX,R_1}}{C_{DOX,core}} = \frac{C_{DOX,R_2}}{C_{DOX,ext}} \tag{5.2.3}$$

Thus, the boundary conditions at R_1 and R_2 are:

$$C_{DOX,mem}\left(r = {R_1}^+, t\right) = KC_{core}(t) \tag{5.2.4}$$

$$C_{DOX,mem}(r = {R_2}^-, t) = KC_{ext}(t) \tag{5.2.5}$$

The steady-state solution to Eq. (5.2.2) is given by:

$$C_{DOX,mem}(r,t) = -\frac{KC_{ext}(t) + KC_{core}(t)}{r\left(\frac{1}{R_1} - \frac{1}{R_2}\right)} + KC_{core}(t) + \frac{KC_{ext}(t) - KC_{core}(t)}{R_1\left(\frac{1}{R_1} - \frac{1}{R_2}\right)} \tag{5.2.6}$$

Although we have solved for the concentration profile of DOX in the bilayer as a function of t and r, the expressions for $C_{ext}(t)$ and $C_{core}(t)$ are still unknown. In order to find $C_{ext}(t)$ and $C_{core}(t)$, a mass balance must be performed on the drug. Since drug is neither created nor degraded at any time t, any DOX released by the core has diffused into the vesicle bilayer at R_1:

$$V_1 \frac{dC_{core}(t)}{dt} = -J\Big|_{r=R1} A_1 \tag{5.2.7}$$

where V_1 is the volume of the inner aqueous core, A_1 is the surface area of the vesicle membrane at R_1, and $J|_{r=R_1}$is the flux at R_1, which is equal to:

$$J|_{r=R_1} = -D_{DOX} \frac{\partial C_{mem}(R_1, t)}{\partial r}\Big|_{r=R_1} = -D_{DOX} \frac{KC_{ext}(t) - KC_{core}(t)}{{R_1}^2 \left(\frac{1}{R_1} - \frac{1}{R_2}\right)} \tag{5.2.8}$$

Combining Eqs. (5.2.7) and (5.2.8) yields:

$$\frac{dC_{core}(t)}{dt} = \frac{A_1 D_{DOX} K}{V_1} \left(\frac{C_{ext}(t) - C_{core}(t)}{{R_1}^2 \left(\frac{1}{R_1} - \frac{1}{R_2}\right)} \right) \tag{5.2.9}$$

A similar analysis is performed at R_2 where any DOX that is gained by the external buffer at any time t has been released from the vesicle bilayer:

$$V_2 \frac{dC_{ext}(t)}{dt} = J\Big|_{r=R2} A_2 \tag{5.2.10}$$

where V_2 is the volume of the external buffer, A_2 is the surface area of the vesicle membrane at R_2, and $J|_{r=R_2}$is the flux at R_2, which is equal to:

$$J|_{r=R_2} = -D_{DOX} \frac{\partial C_{mem}(R_2, t)}{\partial r}\Big|_{r=R_2} = -D_{DOX} \frac{KC_{ext}(t) - KC_{core}(t)}{{R_2}^2 \left(\frac{1}{R_1} - \frac{1}{R_2}\right)} \tag{5.2.11}$$

Combining Eqs. (5.2.10) and (5.2.11) yields:

$$\frac{dC_{ext}(t)}{dt} = -\frac{A_2 D_{DOX} K}{V_2} \left(\frac{C_{ext}(t) - C_{core}(t)}{{R_2}^2 \left(\frac{1}{R_1} - \frac{1}{R_2}\right)} \right) \tag{5.2.12}$$

The ordinary differential equations (ODEs) (5.2.9) and (5.2.12) are coupled as the dependent variables $C_{ext}(t)$ and $C_{core}(t)$ are present in both equations. These two ODEs can be solved by taking the difference of the two differential equations:

$$\frac{d[C_{core}(t)-C_{ext}(t)]}{dt} = \frac{A_1 D_{DOX} K}{V_1}\left(\frac{C_{ext}(t)-C_{core}(t)}{{R_1}^2\left(\frac{1}{R_1}-\frac{1}{R_2}\right)}\right) - \frac{A_2 D_{DOX} K}{V_2}\left(\frac{C_{core}(t)-C_{ext}(t)}{{R_2}^2\left(\frac{1}{R_1}-\frac{1}{R_2}\right)}\right) \quad (5.2.13)$$

To solve this resulting ODE, $C_{core}(t) - C_{ext}(t)$ is defined as a new variable $y(t)$:

$$y(t) \equiv C_{core}(t) - C_{ext}(t) \quad (5.2.14)$$

Equation (5.2.13) then becomes:

$$\frac{dy(t)}{dt} = -\frac{A_1 D_{DOX} K}{V_1}\left(\frac{y(t)}{{R_1}^2\left(\frac{1}{R_1}-\frac{1}{R_2}\right)}\right) - \frac{A_2 D_{DOX} K}{V_2}\left(\frac{y(t)}{{R_2}^2\left(\frac{1}{R_1}-\frac{1}{R_2}\right)}\right) \quad (5.2.15)$$

An initial condition for $y(t)$ is required to complete the solution for $y(t)$. At the beginning of the release, it is assumed that all the DOX is initially present in the aqueous core at a concentration C_0, and DOX is not present in the vesicle membrane nor the external buffer. Therefore, the initial condition for $y(t)$ is:

$$y(t=0) = C_{core}(t=0) - C_{ext}(t=0) = C_0 \quad (5.2.16)$$

Solving Eq. (5.2.15) using the initial condition given by Eq. (5.2.16) results in:

$$y(t) = C_0 \exp\left(-\frac{A_1 D_{DOX} K {R_2}^2 V_2 + A_2 D_{DOX} K {R_1}^2 V_1}{V_1 V_2 {R_1}^2 {R_2}^2\left(\frac{1}{R_1}-\frac{1}{R_2}\right)}\right) \quad (5.2.17)$$

Going back to the definition for $y(t)$ and rearranging for $C_{core}(t)$ yields:

$$C_{core}(t) = C_{ext}(t) + C_0 \exp\left(-\frac{A_1 D_{DOX} K {R_2}^2 V_2 + A_2 D_{DOX} K {R_1}^2 V_1}{V_1 V_2 {R_1}^2 {R_2}^2 \left(\frac{1}{R_1} - \frac{1}{R_2}\right)}\right) \quad (5.2.18)$$

Since we now have a relationship between $C_{core}(t)$ and $C_{ext}(t)$, we can express Eq. (5.2.12) in terms of one dependent variable and solve the ODE:

$$\frac{dC_{ext}(t)}{dt} = \frac{A_2 D_{DOX} K C_0}{V_2 {R_2}^2 \left(\frac{1}{R_1} - \frac{1}{R_2}\right)} \exp\left(-\frac{A_1 D_{DOX} K {R_2}^2 V_2 + A_2 D_{DOX} K {R_1}^2 V_1}{V_1 V_2 {R_1}^2 {R_2}^2 \left(\frac{1}{R_1} - \frac{1}{R_2}\right)}\right) \quad (5.2.19)$$

The initial condition for $C_{ext}(t)$ was that drug was not initially present in the external buffer:

$$C_{ext}(t = 0) = 0 \quad (5.2.20)$$

Integrating Eq. (5.2.19) with the initial condition given by Eq. (5.2.20) gives rise to an expression for the concentration of drug in the external buffer, which represents the released drug:

$$C_{ext}(t) = \frac{A_2 V_1 {R_1}^2 C_0}{A_1 {R_2}^2 V_2 + A_2 {R_1}^2 V_1}\left[1 - \exp\left(-\frac{A_1 D_{DOX} K {R_2}^2 V_2 + A_2 D_{DOX} K {R_1}^2 V_1}{V_1 V_2 {R_1}^2 {R_2}^2 \left(\frac{1}{R_1} - \frac{1}{R_2}\right)} t\right)\right] \quad (5.2.21)$$

From Eq. (5.2.21), we can define the time constant τ_c, which describes how fast the external concentration changes. It is defined as the time it takes for $C_{ext}(t = \tau_c)$ to increase to 63% of its final value:

$$\tau_c \equiv \frac{V_1 V_2 {R_1}^2 {R_2}^2 \left(\frac{1}{R_1} - \frac{1}{R_2}\right)}{A_1 D_{DOX} K {R_2}^2 V_2 + A_2 D_{DOX} K {R_1}^2 V_1} \quad (5.2.22)$$

The mass balance from Eq. (5.2.10) described how much drug leaves the vesicle membrane as a function of time by multiplying the flux by the area. Now that we have an expression for $C_{ext}(t)$, we can determine the amount of drug leaving the vesicle bilayer per time:

$$J|_{r=R2}A_2 = \frac{A_2 C_0 D_{DOX} K}{{R_2}^2\left(\frac{1}{R_1}-\frac{1}{R_2}\right)} \exp\left(-\frac{A_1 D_{DOX} K {R_2}^2 V_2 + A_2 D_{DOX} K {R_1}^2 V_1}{V_1 V_2 {R_1}^2 {R_2}^2\left(\frac{1}{R_1}-\frac{1}{R_2}\right)} t\right) \tag{5.2.23}$$

In order to determine the amount of drug that has left at some time t, we can integrate Eq. (5.2.23) with respect to time from $t = 0$ to the desired time t when the drug release is measured.

$$\begin{aligned} n_{released}(t) &= \int_0^t J|_{r=R2}A_2\, dt \\ &= \frac{A_2 V_1 {R_1}^2 C_0}{A_1 {R_2}^2 V_2 + A_2 {R_1}^2 V_1}\left[1 - \exp\left(-\frac{A_1 D_{DOX} K {R_2}^2 V_2 + A_2 D_{DOX} K {R_1}^2 V_1}{V_1 V_2 {R_1}^2 {R_2}^2\left(\frac{1}{R_1}-\frac{1}{R_2}\right)} t\right)\right] \end{aligned} \tag{5.2.24}$$

Finally, the percent of drug released can be calculated as:

$$\%\, released = \frac{n_{released}(t)}{C_0 V_1} \tag{5.2.25}$$

where $C_0 V_1$ is the initial amount of drug loaded into the aqueous core.

According to the pseudo-steady analysis, it is assumed that the rate of DOX diffusion is very fast while the rate at which the compartment concentrations changes is slow. This criteria can be described in terms of the diffusion time constant and the time constant at which the external concentrations change. Accordingly, in order for the pseudo-steady analysis to be valid, the following criterion must be true: $\tau_d \ll \tau_c$ or $\frac{\tau_d}{\tau_c} \ll 1$, where τ_c was previously defined in Eq. (5.2.22), and τ_d is the diffusional time scale, which is defined as:

$$\tau_d \equiv \frac{(R_2 - R_1)^2}{D_{DOX}} \tag{5.2.26}$$

After taking the ratio of $\frac{\tau_d}{\tau_c}$ and simplifying terms, the ratio $\frac{\tau_d}{\tau_c}$ can be rewritten as:

$$\frac{\tau_d}{\tau_c} = \frac{3K(R_2 - R_1)({R_2}^3 - {R_1}^3)}{{R_1}^2{R_2}^2} \ll 1 \tag{5.2.27}$$

As mentioned above, in order for the pseudo-steady analysis to be valid, Eq. (5.2.27) must hold true. When the parameter values were input into Eq. (27), $\frac{\tau_d}{\tau_c} = 81.8$. Although predictions with this approach were reasonable, 81.8 is much greater than 1, and the required criterion was not satisfied. Therefore, this model was not further pursued.

5.3. MATLAB Code for Method of Lines

The following MATLAB code was used to perform the method of lines. The ode45 solver was used to solve the system of ODES. Two sets of code were used to solve for the release during the Tf-conjugation and the *in vitro* release study.

```
%NUMERICALMETHODS.M

function dcdt = numericalmethods(t,c)
D = 3600*2.5*10^-17;%DOX diffusion coefficient in cm^2/s
K = 10; %partition coefficient
R2 = 80*10^-7;%total Tf-DPEL vesicle radius in cm
R1 = 36.2*10^-7;  %aqueous core radius in cm
h = (R2-R1)/100; %distance between each node in cm
dcdt = zeros(size(c));
dcdt(1) = (D*K) * ( (c(2) - c(1))/h)*(4*pi*R1^2)/((4/3)*pi*R1^3); %mass
balance at R1
for i=2:100
    dcdt(i) = D * ( ((2/(R1+(i-1)*h)) * ( c(i+1)-c(i-1)) / (2*h))  + ( (
c(i+1)-2*c(i)+c(i-1))/h^2) ) ;
end %ODEs at each non-boundary node

dcdt(101) = -(D*K) * ( (c(101) - c(100))/h)*(4*pi*R2^2)/1000; %mass balance
at R2

%SOLVENUMERICALMETHODS.M

K=10 %partition coefficient
```

```
C0=120 %inner aqueous core concentration in ug/mL
a=K*C0 %concentration at node 1 due to partitioning
c0 = [a 0 0 0 0 0 0 0 0 0 0 0 0 0 0 0 0 0 0 0 0 0 0 0 0 0 0 0 0 0 0 0 0 0 0 0
0 0 0 0 0 0 0 0 0 0 0 0 0 0 0 0 0 0 0 0 0 0 0 0 0 0 0 0 0 0 0 0 0 0 0 0 0 0 0
0 0 0 0 0 0 0 0 0 0 0 0 0 0 0 0 0 0 0 0 0 0 0 0 0 0 ]; %initial conditions at
every node in ug/mL
tspan = [0 2 4 6 8 24]; %time points for Tf-conjugation in hours
[t,c] = ode45('numericalmethods',tspan,c0);
D = 3600*2.5*10^-17; %DOX diffusion coefficient in cm^2/s
R2 = 80*10^-7; %total Tf-DPEL vesicle radius in cm
R1 = 36.2*10^-7;  %aqueous core radius in cm
h = (R2-R1)/100; %distance between each node in cm
r = [36.2*10^-7:h:80*10^-7]; %radial distance from center of vesicle for
every node in cm

plot(r,c(1,:),r,c(2,:),r,c(3,:),r,c(4,:),r,c(5,:),r,c(6,:))
legend('t = 0','t = 2','t = 4','t = 6','t = 8','t = 24')
xlabel('Radius (nm)');
ylabel('Concentration (ug/mL)');

%NUMERICALMETHODS2.M

function dcdt = numericalmethods2(t,c)
D = 3600*2.5*10^-17;%DOX diffusion coefficient in cm^2/s
K = 10; %partition coefficient
R2 = 80*10^-7;%total Tf-DPEL vesicle radius in cm
R1 = 36.2*10^-7;  %aqueous core radius in cm
h = (R2-R1)/100; %distance between each node in cm
dcdt = zeros(size(c));
dcdt(1) = (D*K) * ( (c(2) - c(1))/h)*(4*pi*R1^2)/((4/3)*pi*R1^3); %mass
balance at R1
for i=2:100
    dcdt(i) = D * ( ((2/(R1+(i-1)*h)) * ( c(i+1)-c(i-1)) / (2*h))  + ( (
c(i+1)-2*c(i)+c(i-1))/h^2) ) ;
end %ODEs at each non-boundary node

dcdt(101) = -(D*K) * ( (c(101) - c(100))/h)*(4*pi*R2^2)/1000; %mass balance
at R2

%SOLVENUMERICALMETHODS2.M

K = 10 %partition coefficient
c0 = [30.32628823   30.26663843 30.18718631 30.08822688 29.97074448
29.83472828 29.68147601 29.51068646 29.32395289 29.12069897 28.90279506
28.66940477 28.42265686 28.16146972 27.88821147 27.60157006 27.30413373
26.99437459 26.67508168 26.34452576 26.00567734 25.65662023 25.30048706
24.93518907 24.56400182 24.18467816 23.80061765 23.40942889 23.01461668
22.61365946 22.21014891 21.80144723 21.39121498 20.97671196 20.5616501
20.14320053 19.72510948 19.30447296 18.88505507 18.4638901  18.04474411
17.62460293 17.20721931 16.78954363 16.37530077 15.96141845 15.55157978
15.14270238 14.7384144  14.33563566 13.93792688 13.54222205 13.15200279
12.7642289  12.38229195 12.00318885 11.63021099 11.26040328 10.89694749
10.53694709 10.18346561 9.833675117 9.490513081 9.151229764 8.81862948
8.490049835 8.168155648 7.850380501 7.539244127 7.232284195 6.931870493
6.635652349 6.345845464 6.060217836 5.780827641 5.505567994 5.236336784
```

```
4.971158104 4.711767469 4.456325218 4.206403046 3.960302207 3.719429759
3.482231934 3.249950937 3.021181438 2.797001159 2.576156053 2.359560293
2.146113355 1.936567333 1.729976864 1.526933951 1.326649427 1.12955769
0.935026212 0.743334741 0.554007249 0.367172234 0.18250946  2.84E-17]
%initial condition at each node in ug/mL
tspan = [0 2 4 6 8 24 48 72 96 120 144 168 192]; %time points for release
experiment in hours
[t,c] = ode45('numericalmethods2',tspan,c0);
D = 3600*10*10^-17; %DOX diffusion coefficient in cm^2/s
R2 = 80*10^-7; %total Tf-DPEL vesicle radius in cm
R1 = 36.2*10^-7; %aqueous core radius in cm
h = (R2-R1)/100;%distance between each node in cm
r = [36.2*10^-7:h:80*10^-7];  %radial distance from center of vesicle for
every node in cm
n=C0*(4/3)*pi*(R1^3)+((4/3)*pi*(((R1+h)^3)-(R1^3))*a) %drug released
n2=(1000*c(:,101)/K) %initial amount of drug
N=n2./n %percent release

L=[0 2 4 6 8 24 48 72 96 120 144 168 192] %time points for experimental data
f5=[0 0.1231 0.2467 0.3262 0.3313 0.5769 0.6349 0.6721 0.7127 0.7512 0.7884
0.8095 0.8471] %% released for experimental data

plot(t,N,'-',L,f5,'-')
legend('ODE45','Experimental','t = 4 s','t = 6 s','t = 8 s','t = 24 s','t =
72 s','t = 96 s','t = 120 s','t = 144 s','t = 168 s','t = 192
s','Location','best')
xlabel('t (hr)');
ylabel('% released');
axis([ 0 192 0 1])
```

6. Works Cited

[1] R. Siegel, J. Ma, Z. Zou and A. Jemal, "Cancer Statistics, 2014," *CA Cancer J Clin,* pp. 9-29, 2014.

[2] A. Urruticoechea, R. Alemany, J. Balart, A. Villanueva, F. Viñals and G. Capellá, "Recent Advances in Cancer Therapy: An Overview," *Current Pharmaceutical Design,* vol. 16, pp. 3-10, 2010.

[3] J. Figueras, J. Torras, C. Valls, L. Llado, E. Ramos and J. Marti-Rague, "Surgical resection of colorectal liver metastases in patients with expanded indications: a single-center experience with 501 patients," *Dis Colon Rectum,* vol. 50, no. 4, pp. 478-488, 2007.

[4] A. C. Begg, F. A. Stewar and C. Vens, "Strategies to improve radiotherapy with targeted drugs," *Nature Reviews Cancer,* vol. 11, pp. 239-253, 2011.

[5] G. Delaney, S. Jacob, C. Featherstone and M. Barton, "The role of radiotherapy in cancer treatment: estimating optimal utilization from a review of evidence-based clinical guidelines," *Cancer,* vol. 104, no. 6, pp. 1129-1137, 2005.

[6] S. M. Bentzen, "Preventing or reducing late side effects of radiation therapy: radiobiology meets molecular pathology," *Nature Reviews Cancer,* vol. 6, pp. 702-713, 2006.

[7] C. F. Thorn, C. Oshiro, S. Marsh, T. Hernandez-Boussard, H. McLeod, T. E. Klein and R. B. Altman, "Doxorubicin pathways: pharmacodynamics and adverse effects," *Pharmacogenet Genomics,* vol. 21, no. 7, pp. 440-446, 2011.

[8] A. Rahman, N. More and P. S. Schein, "Doxorubicin-induced Chronic Cardiotoxicity and Its Protection by Liposomal Administration," *Cancer Res,* vol. 42, pp. 1817-1825, 1982.

[9] S. K. Sahoo, T. K. Jain, M. K. Reddy and V. Labhasetwar, "Nano-Sized Carriers for Drug Delivery," in *NanoBioTechnology,* Humana Press, 2008, pp. 329-348.

[10] K. Greish, "Enhanced Permeability and Retention (EPR) Effect for Anticancer Nanomedicine Drug Targeting," *Cancer Nanotechnology, Methods in Molecular Biology,* vol. 624, pp. 25-37, 2010.

[11] M. L. Immordino, F. Dosio and . L. Cattel, "Stealth liposomes: review of the basic science, rationale, and clinical applications, existing and potential," *Int J Nanomedicine,* vol. 1, no. 3, pp. 297-315, 2006.

[12] Y. Fan and Q. Zhang, "Development of liposomal formulations: From concept to clinical investigations," *Asian Journal of Pharmaceutical Sciences,* vol. 8, no. 2, pp. 81-87, 2013.

[13] Y. Barenholz, "Doxil®—The first FDA-approved nano-drug: Lessons learned," *Journal of Controlled Release,* pp. 117-134, 2012.

[14] C. Allen, N. Dos Santos, R. Gallagher, G. N. C. Chiu, Y. Shu, M. Li, S. A. Johnstone, A. S. Janoff, L. D. Mayer, M. S. Webb and M. B. Bally, "Controlling the Physical Behavior and Biological Performance of Liposome Formulations through Use of the Surface Grafted Poly(ethylene Glycol)," *Bioscience Reports,* vol. 22, no. 2, pp. 225-250, 2002.

[15] J. P. Jain, W. Y. Ayen and N. Kumar, "Self Assembling Polymers as Polymersomes for Drug Delivery," *Current Pharmaceutical Design,* vol. 17, no. 1, pp. 65-79, 2011.

[16] P. J. Photos, L. Bacakova, B. Discher, F. S. Bates and D. E. Discher, "Polymer vesicles in vivo: correlations with PEG molecular weight," *Journal of Controlled Release,* vol. 90, no. 3, pp. 323-334, 2003.

[17] F. Ahmed, R. I. Pakunlu, A. Brannan, F. Bates, T. Minko and D. E. Discher, "Biodegradable polymersomes loaded with both paclitaxel and doxorubicin permeate and shrink tumors, inducing apoptosis in proportion to accumulated drug," *Journal of Controlled Release,* vol. 116, no. 2, pp. 150-158, 2006.

[18] K. Osada and K. Kataoka, "Drug and Gene Delivery Based on Supramolecular Assembly of PEG-Polypeptide Hybrid Block Copolymers," *Adv. Polym. Sci.,* vol. 202, pp. 113-153, 2006.

[19] K. Wang, H. Dong, H. Wen, M. Xu, C. Li, Y. Li, H. N. Jones, D. Shi and X. Zhang, "Novel Vesicles Self-Assembled From Amphiphilic Star-Armed PEG/Polypeptide Hybrid Copolymers for Drug Delivery," *Macromolecular Bioscience,* vol. 11, no. 1, pp. 65-71, 2011.

[20] E. P. Holowka, D. J. Pochan and T. J. Deming, "Charged polypeptide vesicles with controllable diameter," *J Am Chem Soc.,* vol. 127, no. 35, pp. 12423-12428, 2005.

[21] U. J. Choe, A. R. Rodriguez, Z. Li, S. Boyarskiy, T. J. Deming and D. T. Kamei, "Characterization and Minimization of Block Copolypeptide Vesicle Cytotoxicity Using Different Hydrophobic Chain Lengths," *Macromolecular Chemistry and Physics,* vol. 214, no. 9, pp. 994-999, 2013.

[22] J. N. Israelachvili, Intermolecular and Surface Forces: With Applications to Colloidal and Biological Systems, London/Orlando: Academic Press, 1985.

[23] V. P. Torchilin, T. S. Levchenko, R. Rammohan, N. Volodina, B. Papahadjopoulos-Sternberg and G. G. D'Souza, "Cell transfection in vitro and in vivo with nontoxic TAT

peptide-liposome-DNA complexes," *Proc Natl Acad Sci U S A.,* vol. 100, no. 4, pp. 1972-1977, 2003.

[24] J. D. Puglisi, L. Chen, A. D. Frankel and J. R. Williamson, "Role of RNA structure in arginine recognition of TAR RNA," *Proc Natl Acad Sci U S A.,* vol. 90, no. 8, pp. 3680-3684, 1993.

[25] V. Z. Sun, U. J. Choe, A. R. Rodriguez, H. Dai, T. J. Deming and D. T. Kamei, "Transfection of Mammalian Cells Using Block Copolypeptide Vesicles," *Macromolecular Bioscience,* vol. 13, no. 5, pp. 539-550, 2013.

[26] R. Kircheis, S. Schüller, S. Brunner, M. Ogris, K. H. Heider, W. Zauner and E. Wagner, "Polycation-based DNA complexes for tumor-targeted gene delivery in vivo," *The Journal of Gene Medicine,* vol. 1, no. 2, pp. 111-120, 1999.

[27] U. J. Choe, A. R. Rodriguez, B. S. Lee, S. M. Knowles, M. A. Wu, T. J. Deming and D. T. Kamei, "Endocytosis and Intracellular Trafficking Properties of Transferrin-Conjugated Block Copolypeptide Vesicles," *Biomacromolecules,* vol. 14, no. 5, pp. 1458-1464, 2013.

[28] M. C. Chung, "Structure and Function of Transferrin," *Biochemical Education,* vol. 12, no. 4, pp. 146-154, 2010.

[29] P. Ponka and C. N. Lok, "The transferrin receptor: role in health and disease," *The International Journal of Biochemistry & Cell Biology,* vol. 31, no. 10, pp. 1111-1137, 1999.

[30] C. Dufes, J. M. Muller, W. Couet, J. C. Olivier, I. F. Uchegbu and A. G. Schätzlein, "Anticancer Drug Delivery with Transferrin Targeted Polymeric Chitosan Vesicles," *Pharmaceutical Research,* vol. 21, no. 1, pp. 101-107, 2004.

[31] G. Niu, B. Cogburn and J. Hughes, "Preparation and Characterization of Doxorubicin Liposomes," *Cancer Nanotechnology, Methods in Molecular Biology,* vol. 624, pp. 211-29, 2010.

[32] L. D. Mayer, M. B. Bally and P. R. Cullis, "Uptake of adriamycin into large unilamellar vesicles in response to a pH gradient," *Biochim Biophys Acta,* vol. 857, no. 1, pp. 123-126, 1986.

[33] G. Haran, R. Cohen, L. K. Bar and Y. Barenholz , "Transmembrane ammonium sulfate gradients in liposomes produce efficient and stable entrapment of amphiphatic weak bases," *Biochimica et Biophysica Acta,* vol. 1151, pp. 201-215, 1993.

[34] D. D. Lasic, P. M. Frederik, M. A. Stuart, Y. Barenholz and T. J. McIntosh, "Gelation of liposome interior: A novel method for drug encapsulation," *FEBS,* vol. 312, pp. 255-258,

1992.

[35] G. Gregoriadis, Liposome Technology: Entrapment of Drugs and Other Materials into Liposomes, CRC Press, 2006.

[36] T. J. Deming, "Facile synthesis of block copolypeptides of defined architecture," *Nature,* vol. 390, pp. 386-389, 1997.

[37] Y. H. Bae and K. Park, "Targeted drug delivery to tumors: Myths, reality and possibility," *Journal of Controlled Release,* vol. 153, pp. 198-205, 2011.

[38] J. Rejman, V. Oberle, I. S. Zuhorn and D. Hoekstra, "Size-dependent internalization of particles via the pathways of clathrin- and caveolae-mediated endocytosis," *The Biochemical Journal,* vol. 377, pp. 156-169, 2004.

[39] N. Dos Santos, K. A. Cox, C. A. McKenzie, F. van Baarda, R. C. Gallagher, G. Karlsson, K. Edwards, L. D. Mayer, C. Allen and M. B. Bally, "pH gradient loading of anthracyclines into cholesterol-free liposomes: enhancing drug loading rates through use of ethanol," *Biochim Biophys Acta,* vol. 1661, pp. 47-60, 2004.

[40] S. Dashi, P. N. Murthy, L. Nath and P. Chowdhury, "Kinetic Modeling On Drug Release From Controlled Drug Delivery Systems," *Acta Poloniae Pharmaceutica - Drug Research,* vol. 67, no. 3, pp. 217-223, 2010.

[41] D. Y. Arifin, L. Y. Lee and C. Wang, "Mathematical modeling and simulation of drug release from microspheres: Implications to drug delivery systems," *Advanced Drug Delivery Reviews,* vol. 58, pp. 1274-1325, 2006.

[42] S. Modi and B. D. Anderson, "Determination of Drug Release Kinetics from Nanoparticles: Overcoming Pitfalls of the Dynamic Dialysis Method," *Mol. Pharmaceutics,* vol. 10, pp. 3076-3089, 2013.

[43] A. Choucair, P. L. Soo and A. Eisenberg, "Active Loading and Tunable Release of Doxorubicin from Block Copolymer Vesicles," *Langmuir,* vol. 21, pp. 9308-9313, 2005.

[44] J. M. Frazier, In-Vitro Toxicity Testing: Applications to Safety Evaluation, CRC Press, 1992.

[45] E. Borenfreund, H. Babich and N. Martin-Alguacil, "Comparisons of two in vitro cytotoxicity assays—The neutral red (NR) and tetrazolium MTT tests," *Toxicology in Vitro,* vol. 2, no. 1, pp. 1-6, 1988.

[46] M. V. Berridge, P. M. Herst and A. S. Tan, "Tetrazolium dyes as tools in cell biology: New insights into their cellular reduction," *Biotechnol Annu Rev*, vol. 11, pp. 127-152, 2005.

[47] H. N. Keer, J. M. Kozlowski, Y. C. Tsai, C. Lee, R. N. McEwan and J. T. Grayhack, "Elevated transferrin receptor content in human prostate cancer cell lines assessed in vitro and in vivo," *J Urol.*, vol. 143, no. 2, pp. 381-385, 1990.